Using palaeomagnetism to determine late Mesoproterozoic palaeogeographic history and tectonic relations of the Sinclair terrane, Namaqua orogen, Namibia

J. E. PANZIK[1,2]*, D. A. D. EVANS[1], J. J. KASBOHM[3], R. HANSON[4],
W. GOSE[5] & J. DESORMEAU[6]

[1]*Department of Geology and Geophysics, Yale University, 210 Whitney Avenue,
New Haven, CT 06511, USA*

[2]*Department of Earth and Planetary Sciences, University of Tennessee, 1412
Circle Drive, Knoxville, TN 37996, USA*

[3]*Department of Geosciences, Princeton University, Guyot Hall, Princeton, NJ 08544, USA*

[4]*School of Geology, Energy, and the Environment, Texas Christian University,
TCU Box 298830, Fort Worth, TX 76129, USA*

[5]*Department of Geological Sciences, University of Texas at Austin, 2275
Speedway Stop C9000, Austin, TX 78712, USA*

[6]*Geological Sciences and Engineering, University of Nevada, 1664 N. Virginia Street,
Reno, NV 89557, USA*

Corresponding author (e-mail: jpanzik@utk.edu)

Abstract: The Sinclair terrane is an important part of the Namaqua orogenic province in southern Namibia containing well-preserved Mesoproterozoic volcano-sedimentary successions suitable for palaeomagnetic and geochronological studies. The Guperas Formation in the upper part of the Sinclair stratigraphic assemblage contains both volcanic and sedimentary rocks cut by a bimodal dyke swarm with felsic members dated herein by U–Pb on zircon at *c.* 1105 Ma. Guperas igneous rocks yield a pre-fold direction and palaeomagnetic pole similar to that previously reported. Guperas sedimentary rocks yield positive conglomerate and fold tests, with a maximum concentration of characteristic remanence directions at 100% untilting. The combined Guperas data generate a palaeomagnetic pole of 69.8° N, 004.1° E ($A_{95} = 7.4°$, $N = 9$). The 1105 Ma post-Guperas dykes yield stable remanence directions with positive baked-contact tests and a palaeomagnetic pole at 62.3° N, 031.9° E ($A_{95} = 6.9°$, $N = 26$), which is coincident with that of the Kalahari-wide Umkondo large igneous province, demonstrating tectonic coherence of the Sinclair terrane with the Kalahari craton at the time of dyke emplacement. These results show that palaeomagnetic and geochronological studies of the Sinclair terrane can provide kinematic constraints on the tectonic evolution of the Namaqua–Natal–Maud orogenic belt and its role in the formation of the Rodinia supercontinent.

Models for the complex, polycyclic development of the Mesoproterozoic Namaqua–Natal–Maud orogen (NNMO), in southern Africa and formerly adjacent regions of Antarctica, typically involve accretion of island arcs and microcontinental blocks against the Kalahari craton margin, followed by collision with one of the other cratons making up Rodinia (Dalziel *et al.* 2000; Cornell *et al.* 2006; Jacobs *et al.* 2008). Such models can in principle be tested using palaeomagnetism, but this approach is precluded in most parts of the NNMO because of the high metamorphic grade of the rocks. The Sinclair terrane, in southern Namibia (Fig. 1), is the most suitable tectonic element within the NNMO for palaeomagnetic studies of the Mesoproterozoic rocks, because it contains several volcano-sedimentary successions of subgreenschist metamorphic grade (Miller 2008). Robust, well-dated palaeomagnetic poles from Sinclair rocks should provide important constraints on tectonic models for the NNMO, and also may be of use in general models for Rodinia assembly.

Unconformity-bounded successions of Mesoproterozoic volcano-sedimentary rocks within the
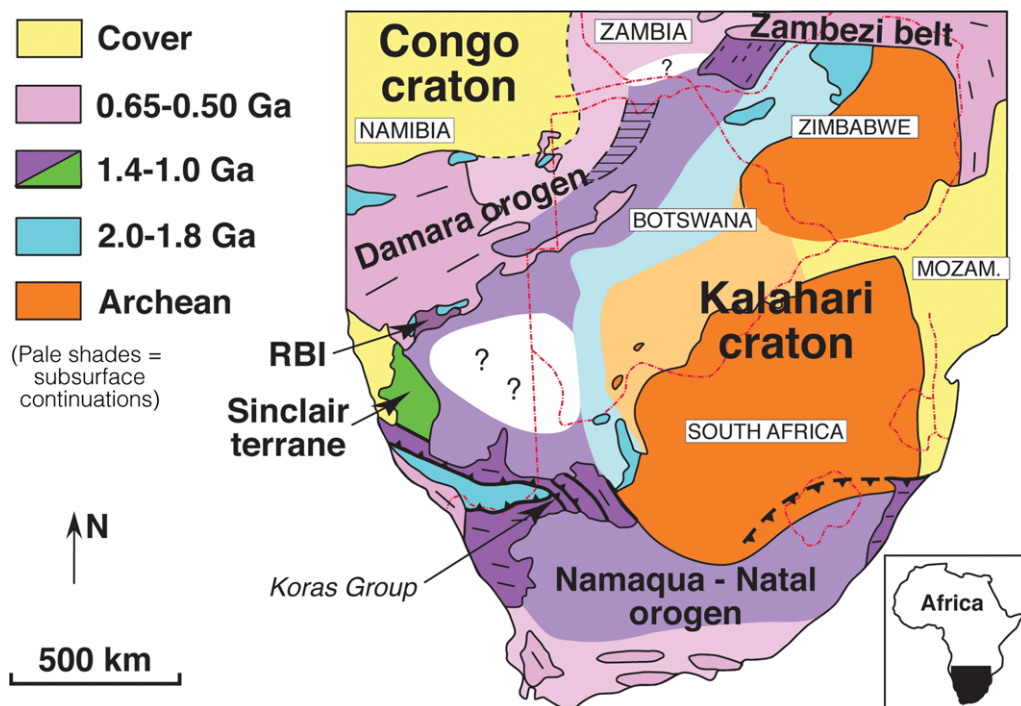
Fig. 1. Simplified tectonic map of southern Africa, modified from Hanson (2003). RBI, Rehoboth basement inlier.

Sinclair terrane are included within the Konkiep Group (Miller 2008). The highest unit, the Aubures Formation, comprises red-brown terrestrial sedimentary rocks, unconformably overlying all other Konkiep units. Among those, the stratigraphically highest succession, the Guperas Formation, contains sandstone and conglomerate, felsic lavas and hypabyssal intrusions, and rare mafic lavas. The Guperas Formation and other parts of the Sinclair terrane were intruded by a bimodal dyke swarm that is truncated by the unconformity at the base of the Aubures Formation.

An early palaeomagnetic study by Piper (1975) was performed on the Sinclair succession using analysis of data at either the natural remanent magnetization (NRM) step or following limited alternating field demagnetization. From the uppermost Precambrian unit in the succession, the Aubures Formation, Piper's (1975) results were broadly reproduced in subsequent research by Kasbohm *et al.* (2015). Piper (1975) sampled several flow units within the Guperas Formation, possibly belonging to one brief eruptive episode based on the absence of sedimentary horizons, collected from four sites within a single, small outcrop area that was revisited in this study (along with other Guperas localities). alternating field demagnetization to 300 Oe yielded

a mean direction to the NW and shallowly upward. It remains unclear whether the magnetization in these rocks is primary, dating from the initial cooling of the lavas, and also whether the four sampled sites adequately average secular variation of the Earth's ancient geodynamo. More measurements on additional sites, including field stability tests, were needed to bolster or refine the Guperas result originally obtained by Piper (1975).

Geological background

The Sinclair terrane preserves low-grade metasedimentary and metavolcanic rocks of Mesoproterozoic age near the western margin of the Kalahari craton (Fig. 1; Hoal 1993; Miller 2008). The shallow level of surface exposure of the Sinclair terrane is anomalous relative to the generally more deeply metamorphosed Precambrian terranes (e.g. Becker *et al.* 2005, 2006; Miller 2013) to the immediate NE (Rehoboth inlier) and south (Namaqualand metamorphic complex). The Sinclair terrane forms an important tectonic element within the Mesoproterozoic NNMO that rims the entire southern margin of the Kalahari craton (including its original extension into Antarctica). This orogen represents

one of the main convergent boundaries active during late Mesoproterozoic assembly of the Rodinia supercontinent, and an understanding of its tectonic evolution is crucial for unravelling the details of Rodinia assembly.

The Konkiep Group within the Sinclair terrane has been shown to have evolved in four prominent magmatic and sedimentary cycles (Watters 1974, 1977; Hoal 1989; Becker *et al.* 2006; Miller 2008, 2013). The first Sinclair cycle is represented by metavolcanic and metasedimentary rocks of the Kairab Formation and associated intrusive rocks (Miller 2008, 2013). The second cycle is represented by the Haremub/Tumuab/Kotzerus granite and granodiorite intrusions and the Nagatis Formation, which consists of shale, arkose, minor basaltic lava and abundant rhyolitic extrusives. The third cycle is partly recorded by the Kunjas Formation (grit, shale, arkose and quartzarenite), and the overlying Haiber Flats, Barby and Welverdiend Formations. These formations are correlative with each other and comprise basaltic to rhyolitic extrusive rocks. A variety of plutonic rocks ranging from gabbro to granite and syenite were also emplaced during this third cycle. The fourth cycle includes the Sonntag Granite and bimodal dyke swarms, and the Guperas Formation of rhyolitic extrusives and basic lava underlain by or intercalated with sandstone and conglomerates. These rocks are unconformably overlain by red sandstones, breccias, conglomerates and siltstones of the Aubures Formation, which is up to 2.6 km thick (Miller 1969; Watters 1974).

Reliable age constraints on Sinclair igneous rocks and the Aubures Formation have in the past been sparse. Volcanic and plutonic rocks in the northern part of the Sinclair terrane have recently yielded U–Pb zircon ages of 1359–1105 Ma (Cornell *et al.* 2015), but how some of the dated rocks correlate with the main part of the terrane farther south remains unclear. Hoal & Heaman (1995) showed that earlier Rb–Sr determinations in the Awasib Mountain area were unreliable, and they provided a U–Pb zircon age of *c.* 1380 Ma for tonalite gneiss related to the first Sinclair cycle as defined above. Felsic intrusive rocks emplaced as part of the first cycle in other parts of the Sinclair terrane have yielded zircon ages of *c.* 1380 and 1330 Ma (Miller 2008, 2013). Available U–Pb zircon ages summarized by Miller (2008, 2013) constrain the second and third Sinclair cycles to have occurred between *c.* 1330 and 1220 Ma. Igneous rocks emplaced at *c.* 1220 Ma have also been found extensively in the Rehoboth region (Becker *et al.* 2005, 2006), but additional magmatic activity in that region at *c.* 1100 Ma (ibid.) suggests the possibility that the fourth Sinclair cycle (Guperas Formation and related rocks) could also have

been emplaced at *c.* 1100 Ma. Magmatism in the Sinclair and Rehoboth terranes in this time frame is likely to correlate with the widespread Umkondo large igneous province (Hanson *et al.* 2004). The Umkondo province is an important lithostratigraphic marker across the Kalahari craton and has yielded a key palaeomagnetic pole (Gose *et al.* 2006) for a relative global Kalahari reconstruction and relative to other Mesoproterozoic cratons. Horstmann *et al.* (1990) reported a K–Ar date of *c.* 1170 Ma for detrital muscovite in the Aubures Formation, providing a maximum age limit for that unit, but a better constraint is now provided by U–Pb laser-ablation inductively coupled plasma mass spectrometry analyses on detrital zircons, with a youngest population of grains at 1108 ± 9 Ma (Kasbohm *et al.* 2015).

Various alternative tectonic models have been proposed for the Sinclair region, including a rift or aulacogen (Kröner 1977; Borg 1988), a back-arc or suprasubduction setting (Hoal 1987, 1993), a collision-related pull-apart basin (Jacobs *et al.* 1993) and a post-collisional extensional collapse (Kampunzu *et al.* 1998). A mantle plume has been implicated for at least part of the magmatism (Hanson *et al.* 2004). More recently, Miller (2008, 2013) has proposed that igneous rocks in the first Sinclair cycle formed in a volcanic arc above a subduction zone dipping to the SW (in present coordinates) and were accreted to the Kalahari craton after *c.* 1330 Ma. Miller (2013) suggests that a switch in subduction polarity caused formation of the second and third Sinclair cycles in arc-related settings along an active continental margin established on top of the earlier accreted arc. Most of these models consider the Sinclair terrane to be autochthonous to the Kalahari craton throughout much of its history, but the back-arc basin model requires at least some post-depositional convergence of unknown magnitude toward the craton. It should also be noted that the Sinclair terrane is delimited to the NE by a pronounced NW-trending subsurface aeromagnetic lineament in Namibia termed the Namaqua front (Corner 2008; Miller 2008, 2013). In addition, the northernmost exposed parts of the Sinclair terrane are deformed by the ductile, 15 km-wide Nam shear zone, (Becker *et al.* 2006; Miller 2008). The nature and magnitude of possible tectonic transport along or across the Namaqua front and the Nam shear zone are unclear. Kasbohm *et al.* (2015) found concordance between palaeomagnetic poles of the Aubures Formation and lithostratigraphically similar Koras Group, the latter deposited definitively on parts of the Namaqua belt that had already been accreted to the Kalahari craton in South Africa, supporting a largely autochthonous position of the Sinclair terrane at *c.* 1100 Ma.

Methods

The geological context of the sample sites is shown in Figures 2 and 3. We collected both cores, using a portable gas-powered drill that has a water-cooled diamond-tipped bit of 2.5 cm diameter, and oriented block samples. Cores are typically 10 cm in length.

The orientation of samples was determined using a sun compass and a Brunton compass mounted on a cylindrical dip gauge. At each dyke and lava flow locale, eight samples were collected, spanning the width of the dyke or the thickness of the lava flow exposure. Sedimentary stratigraphic sections were sampled at one block or core per layer defined by
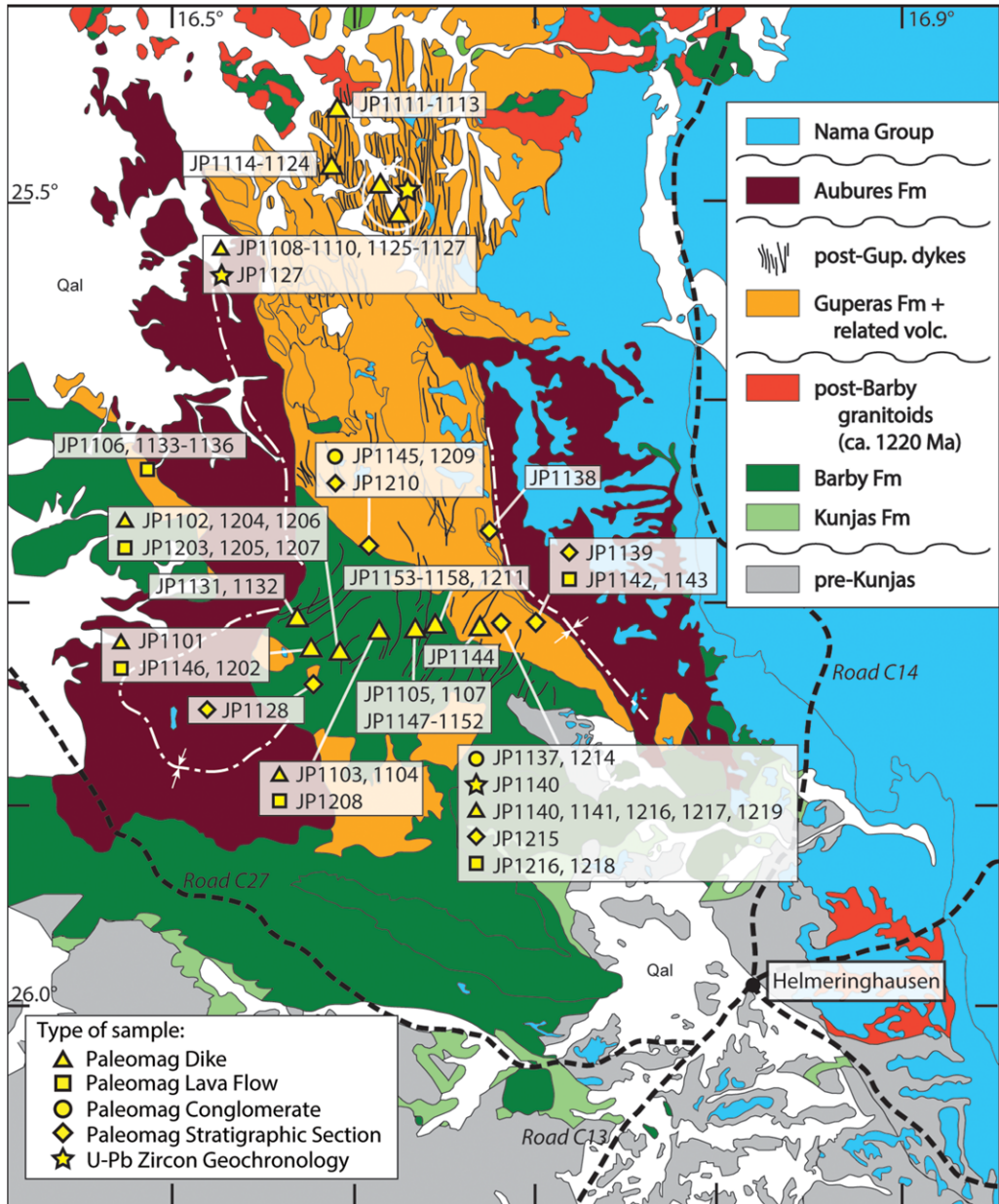

Fig. 2. Geological map of part of the Sinclair terrane, south-central Namibia (after Kasbohm *et al.* 2015). Qal, Quaternary alluvium. Location of Sinclair terrane in regional perspective is shown in Figure 1.
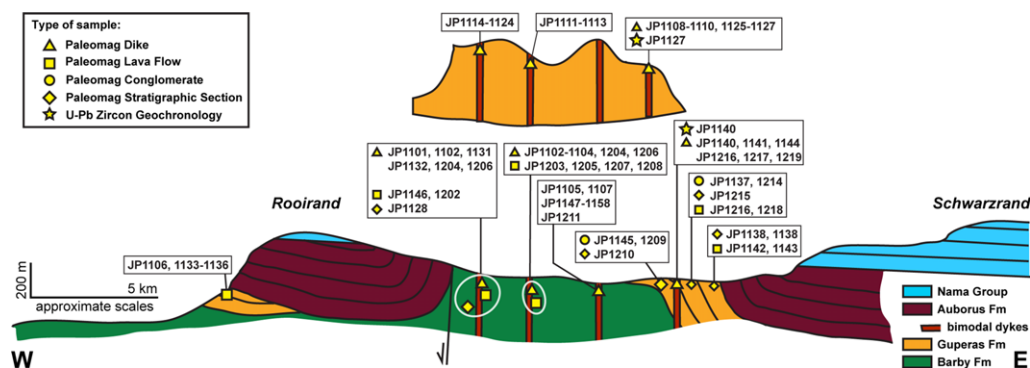
Fig. 3. Simplified and schematic cross-sections of the Sinclair region: top, northern sampling area; bottom, southern area. Modified from Kasbohm *et al.* (2015). Post-Guperas dykes are too numerous to show individually, and thus are represented schematically by geographic region.

distinct depositional boundaries (typically at spacing of several decimetres to metres). The bedding attitude, stratigraphic height and lithology were also recorded for each sample in the stratigraphic sequences. For conglomerate field stability test sites, 20 samples were taken from clasts, with some clasts being sampled twice, and 10 samples from the surrounding matrix. Baked contact tests were sampled in the host rock away from the dykes to a distance greater than the width of the dyke when possible.

The samples were measured in the Yale Paleomagnetic Laboratory in a superconducting quantum interference device (SQuID) magnetometer. Samples were measured for NRM, and then underwent a liquid nitrogen immersion step, and thermal demagnetization was used to systematically remove unstable magnetic overprints to isolate the primary magnetic directions. Thermal demagnetization in 15 or more steps was carried out to *c.* 580 or *c.* 690°C depending on whether the primary magnetization carrier was either magnetite or hematite, respectively.

Samples for U−Pb zircon geochronology were collected at rhyolite dyke localities in which palaeomagnetic sampling was performed. In particular, sites were chosen based on their relatively coarse grain sizes and freshness of surface exposure. Sample JP1127X is from a north−south-striking, steeply west-dipping, 50−60 m-wide, pink, quartz- and feldspar−phyric rhyolite porphyry dyke in the northern part of the study area (Fig. 2). Sample JP1140X is from a NE−SW-striking, steeply dipping, 12 m-wide rhyolite porphyry dyke of similar lithology in the southern part of the study area. Both dykes intrude sedimentary rocks of the Guperas Formation.

Zircon was extracted from the dyke samples using standard rock-crushing and mineral-separation procedures. The study utilized high precision single-grain U−Pb isotope-dilution thermal ionization mass spectrometry (ID-TIMS) following the chemical-abrasion procedures of Mattinson (2005). Chemical abrasion is designed to remove the high-U zones of the zircon susceptible to Pb loss, and in turn, minimize or eliminate Pb-loss correction (Mattinson 2005). Each ID-TIMS result presented represents a single grain that has undergone a 12 h leach at 220°C. ID-TIMS analyses that define a single population are reported as $^{206}Pb/^{238}U$ Th-corrected weighted mean dates. The U−Pb ID-TIMS zircon analyses are provided in Table 1. All reported uncertainties within the text, data table and figure are at the 2σ or 95% confidence level.

Zircons were selected from the post-Guperas dykes based on colour and morphology (i.e. prismatic, euhedral); in general, clear, inclusion-free grains were targeted. Chemical abrasion involved annealing the grains at 900°C for 60 h and then placing the individual grains in 300 μl Teflon FEP capsules containing 75 μl HF at 180°C for 9−12 h to dissolve inclusions and/or radiation-damaged portions of the grains (Mattinson 2005). The leached grains were rinsed and sonicated in a series of steps involving H_2O, 6 N HCl and 3 N HNO_3. After rinsing, the grains were dissolved in 75 μL full-strength HF with a mixed $^{205}Pb-^{233}U-^{235}U$ tracer at 220°C for 48 h. The dissolved grains were dried to salts and then redissolved at 180°C for 12 h in 75 μl 6 N HCl. Prior to adding the solutions to the columns, the 6 N HCl solution was dried to salts and then redissolved in 50 μl 3 N HCl. Pb and U were extracted from the dissolved grains by a HCl-based single-column anion exchange procedure modified after Krogh (1973). The dried Pb and U mixture was dissolved in silica gel (Gerstenberger & Haase 1997) and loaded onto a degassed Re filament for analysis by TIMS using the MIT VG Sector 54 and X62 multi-collector

Table 1. *Zircon U–Pb ID-TIMS isotopic data from post-Guperas dykes*

Fraction zircon	Dates (Ma)								Composition					Isotopic ratios						Correlation coefficients
	$^{206}Pb/^{238}U$ <Th> [a]	±2σ abs	$^{207}Pb/^{235}U$ [b]	±2σ abs	$^{207}Pb/^{206}Pb$ <Th> [a]	±2σ abs	Correlation coefficient	% disc [c]	Pb* (pg) [d]	Pbc (pg) [e]	Pb*/ Pbc [f]	Th/U [g]	$^{206}Pb/^{204}Pb$ [h]	$^{206}Pb/$ ^{238}U [i]	±2σ %	$^{207}Pb/$ 235U [i]	±2σ %	$^{207}Pb/$ ^{206}Pb [i]	±2σ %	$^{206}Pb/^{238}U$ <Th>– $^{207}Pb/^{235}U$
JP1127X																				
z1	1104.96	0.84	1105.3	1	1106.0	2.1	0.718	0.11	35.4	0.17	205.73	0.42	12 415	0.18696	0.082	1.9700	0.15	0.076456	0.10	0.72
z3	1105.6	1.9	1104.6	2.5	1102.5	5.9	0.612	−0.26	9.71	0.20	49.51	0.42	3004	0.18709	0.19	1.9679	0.37	0.07632	0.29	0.61
z4	1105.34	0.69	1106.1	1.3	1107.6	3.4	0.466	0.23	18	0.17	107.43	0.45	6446	0.18703	0.067	1.9723	0.19	0.07632	0.17	0.47
z5	1106.04	0.68	1107.5	1	1110.3	2.5	0.581	0.40	20.9	0.20	105.34	0.45	6324	0.18716	0.067	1.9763	0.15	0.076620	0.12	0.58
JP1140X																				
z1	1110.9	2.2	1108.8	1.8	1104.6	2.8	0.849	−0.56	34.3	0.35	99.11	0.65	5674	0.18806	0.22	1.9802	0.27	0.07640	0.14	0.85
z2	1108.6	2.1	1106.2	2.8	1101.6	7.1	0.523	−0.62	7.92	0.18	44.84	0.56	2633	0.18763	0.20	1.9727	0.41	0.07629	0.35	0.52
z3	1109.6	2.9	1109.0	3.1	1107.9	6.7	0.674	−0.13	17.8	0.50	35.62	0.51	2119	0.18781	0.28	1.9809	0.45	0.07653	0.33	0.67
z4	1105.54	0.73	1105.9	1.2	1106.6	2.8	0.725	0.12	24.4	0.22	112.7	0.44	6773	0.18707	0.072	1.9718	0.18	0.07648	0.13	0.73
z5	1105.41	0.64	1105.9	1	1106.9	2.4	0.679	0.16	22.5	0.21	106.85	0.47	6386	0.18704	0.063	1.9718	0.15	0.076492	0.11	0.68

[a] Corrected for initial Th/U disequilibrium using radiogenic ^{208}Pb and Th/U [magma] = 2.8000.
[b] Isotopic dates calculated using the decay constants 238 = 1.55125×10^{-10} and 235 = 9.8485×10^{-10} (Jaffey *et al.* 1971).
[c] % discordance = $100 - [100 \times (^{206}Pb/^{238}U \text{ date})/(^{207}Pb/^{206}Pb \text{ date})]$.
[d] Total mass of radiogenic Pb.
[e] Total mass of common Pb.
[f] Ratio of radiogenic Pb (including ^{208}Pb) to common Pb.
[g] Th contents calculated from radiogenic ^{208}Pb and the $^{207}Pb/^{206}Pb$ date of the sample, assuming concordance between U–Th and Pb systems.
[h] Measured ratio corrected for fractionation and spike contribution only.
[i] Measured ratios corrected for fractionation, tracer and blank.

mass spectrometers. Pb isotopes were measured by peak-jumping on a Daly detector. U was measured as UO_2^+ with masses 270, 267 and 265 in the axial, H2 and H1 Faraday collectors, respectively. Pb isotope fractionation was corrected based on repeat analyses of NBS981 using a value of 0.25%/amu. Use of the $^{233}U-^{235}U$ double spike allows real-time correction for U fractionation.

Following data acquisition, all measurements were evaluated statistically using Tripoli and U_Pb Redux software (Bowring *et al.* 2011; McLean *et al.* 2011). All dates were calculated using the decay constants of Jaffey *et al.* (1971). All ^{204}Pb was assumed to be from laboratory blank and the data were corrected using measured laboratory blank isotopic compositions, which are based on long-term reduced total procedural blank analyses. The composition used was $^{206}Pb/^{204}Pb = 18.416 \pm 0.349$ (1σ), $^{207}Pb/^{204}Pb = 15.358 \pm 0.226$ and $^{208}Pb/^{204}Pb = 37.46 \pm 0.735$. The zircon analyses have been corrected for ^{230}Th disequilibrium by assuming a magma Th/U ratio of 2.8. The zircon data are presented in Figure 4 and in Table 1.

Results: geochronology

Four zircons from the northern sample JP1127X yielded a $^{206}Pb/^{238}U$ weighted-mean date of 1105.5 ± 0.4 Ma (MSWD = 1.5; Fig. 4; Table 1). The southern sample JP1140X yielded five zircons with $^{206}Pb/^{238}U$ dates ranging from 1110.9 ± 2.2 to 1105.4 ± 0.6 Ma. The three oldest of those five analyses are interpreted as xenocrystic, whereas the two youngest grains yield a $^{206}Pb/^{238}U$ weighted-mean date of 1105.5 ± 0.5 Ma; this age

and that of the northern sample are interpreted as crystallization ages for the dykes. The two crystallization ages are identical, overlapping within uncertainty; yet as will be discussed below, they represent two distinct polarity states of the Mesoproterozoic geomagnetic field.

Results: palaeomagnetism

Guperas igneous rocks

In the northern sampling region, the sampled lava flows (JP1106, 1133–1136) are mafic in composition (no felsic flows were observed in the sampling area), vesicular and each on the order of one to several metres thick. As noted by Piper (1975), palaeomagnetically stable, deuteric hematite is a common constituent of the opaque mineralogy. These sites, on Ganaams Farm, are in the same region where Piper (1975) collected his Guperas lava samples; correlation with the type locality of the Guperas Formation is based on the stratigraphic position of the lavas between underlying Barby Formation mafic lavas and overlying Aubures Formation redbeds. In the southern region, which is the type locality on Guperas Farm, two sites are in massive rhyolites (JP1142, 1143) that occur concordantly within a sandstone-dominated sedimentary section and may be either flow units or hypabyssal intrusions. In all, the Guperas igneous rocks from both regions show excellent stability to thermal demagnetization (Fig. 5). After removal of a low-coercivity and low-unblocking-temperature present-field (north, upward) component probably held as a viscous remanent magnetization and weathering-related

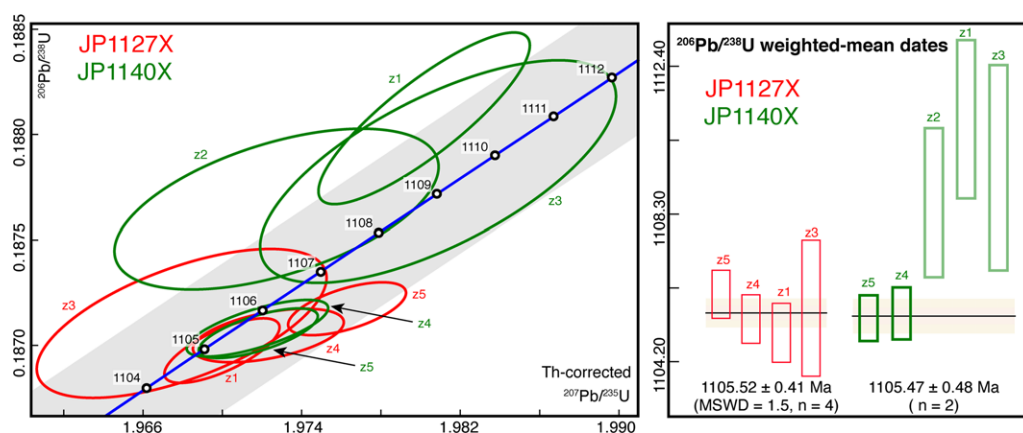**Fig. 4.** Concordia diagram and $^{206}Pb/^{238}U$ (Th-corrected) weighted-mean plot showing the U–Pb zircon analyses from the Post-Guperas dykes. Each ellipse and vertical bar represents a single zircon analysis and the 2σ uncertainties. Individual zircon analysis for JP1127X and JP1140X are distinguished by the colours red and green, respectively. The ages listed on concordia are in Ma.
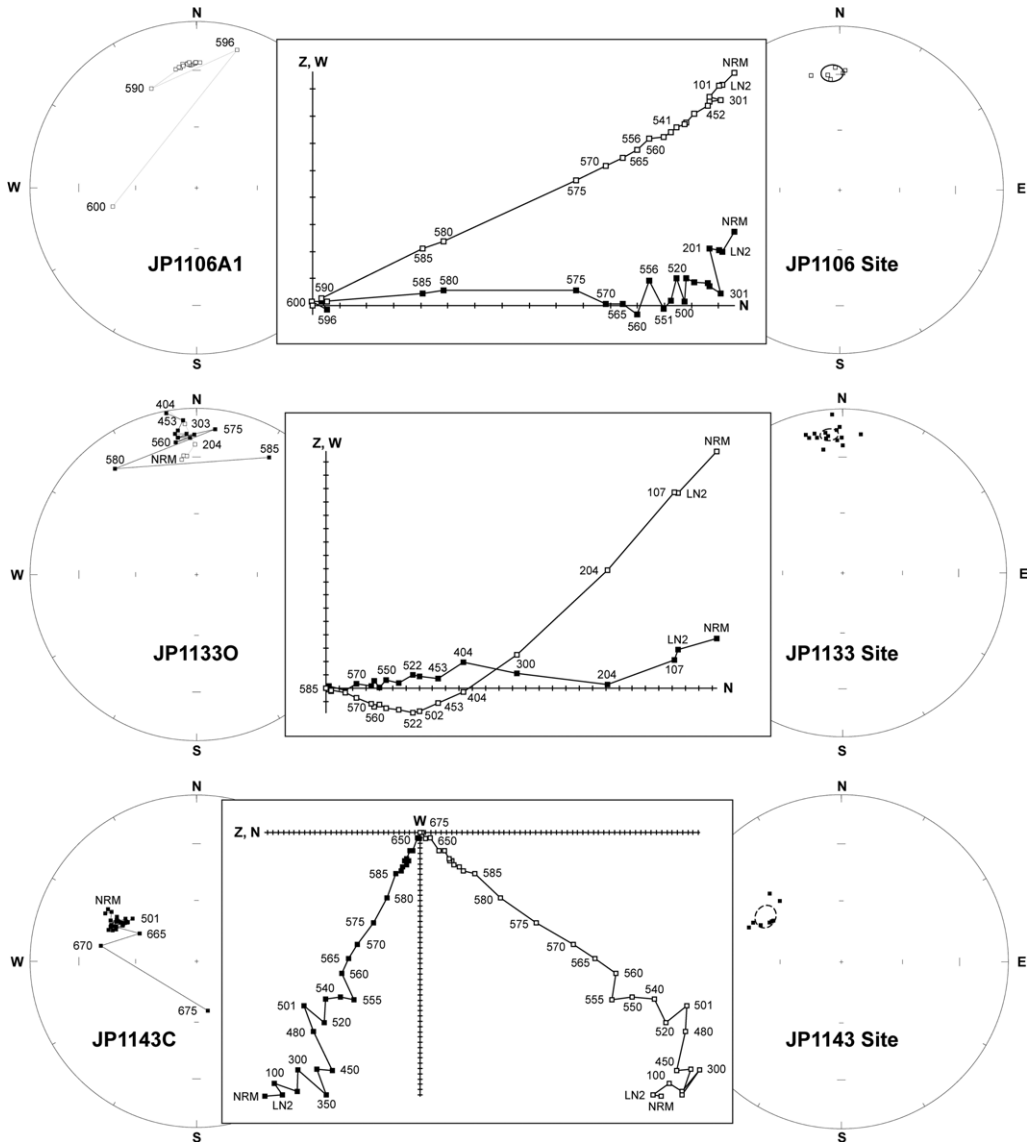
Fig. 5. Typical demagnetization behaviour for Guperas Formation lava flows. Each panel contains an orthogonal projection diagram and an equal-area stereograph. On the orthogonal projection, solid and open symbols represent the horizontal v. vertical plane, respectively, while they represent lower and upper hemisphere, respectively, on the equal area stereograph. All data are shown in geographic coordinates. NRM, natural remanent magnetization. LN2, measurement following immersion in liquid nitrogen. Thermal demagnetization steps labelled in °C.

chemical remanent magnetization, samples there-after exhibited single-component behaviour, with narrow unblocking temperature ranges correspond-ing to the Curie temperatures of stoichiometric magnetite and hematite. Some sites showed un-blocking at both of those intervals, but their dema-gnetization vectors were collinear and analysed

as a single characteristic remanent magnetization (ChRM) component. Most sites exhibited excellent clustering of ChRM directions (Table 2).

Angular breccia clasts, with compositions iden-tical to the underlying coherent basaltic flow unit, were sampled as part of site JP1133. The clasts did not have ChRM directions uniformly

Table 2. *Summary of palaeomagnetic data from all Guperas Formation localities*

	Locality		Average bedding			Geographic Coordinates				100% Tilt-Corrected				VGP			
Code	Latitude (°S)	Longitude (°E)	RHS (deg)	Dip (deg)	n/N	D (deg)	I (deg)	k	α_{95} (deg)	D (deg)	I (deg)	k	α_{95} (deg)	Latitude (°N)	Longitude (°E)	K	A_{95} (deg)
Lavas																	
JP1106	−25.636	016.481	319	20	6/6	356.3	−29.1	198.7	4.8	347.0	−43.5	198.7	4.8	78.2	284.8		
JP1133	−25.638	016.477	319	20	15/16	354.5	16.3	113.6	3.6	356.3	01.2	113.6	3.6	63.5	008.2		
JP1134	−25.636	016.479	319	20	8/8	356.4	−15.0	76.2	6.4	351.4	−29.9	76.2	6.4	77.5	335.1		
JP1135	−25.636	016.480	319	20	7/8	359.4	−17.8	49.5	8.7	354.0	−33.2	49.5	8.7	80.7	338.8		
JP1136	−25.636	016.483	319	20	8/8	003.5	−19.9	270.7	3.4	358.1	−36.0	270.7	3.4	84.1	358.9		
JP1142	−25.706	016.698	307	110		Scattered				Scattered							
JP1143	−25.707	016.696	307	110	8/8	300.9	46.1	97.9	5.3	334.0	−21.0	97.9	5.3	68.2	357.1		
Mean	*N = 6*				52/54	351.5	−04.4	05.6	31.0	350.1	−27.5	21.5	14.8	76.0	333.5	43.0	10.3
Piper (1975) Guperas Lavas																	
84					5	337	−20	37	12					64	318		
85					4	337	−20	28	17					64	318		
86					4	338	−18	342	5					64	321		
87					3	332	−21	140	10					60	311		
Mean	*N = 4*					336.4	−19.9	871.0	3.1					62.9	316.6		
Sediments																	
JP1128	−25.736	016.579	263	52	7/12	023.9	63.8	11.8	18.3	006.0	17.7	15.4	15.9	54.7	026.9		
JP1138	−25.665	016.674	110	13	12/12	006.7	−17.7	16.8	10.9	007.3	−05.0	16.8	10.9	65.8	034.7		
JP1139	−25.707	016.697	308	110	16/18	301.4	44.3	22.4	8.0	353.5	−07.7	16.3	9.4	67.3	359.8		
Mean	*N = 3*				35/42	349.5	36.4	02.4	108.2	002.1	00.2	28.8	23.4	63.3	021.7	60.5	16.0
Sample Mean	*N = 35*				35/42	340.0	32.8	03.1	16.5	000.7	−01.8	12.8	7.1	65.3	018.7	19.3	5.7
Combined																	
Mean	*N = 9*				87/96	351.0	7.5	03.8	30.4	354.5	−17.8	13.4	14.6	74.0	356.8	30.8	9.4

RHS, Right-hand strike; D, mean declination; I, mean inclination; k, K, Fisher's (1953) precision parameter; α_{95}, A_{95}, radius of the 95% confidence cone; VGP, virtual geomagnetic pole. Piper's (1975) results for Guperas Formation lava flows were added for comparison, but not used in our computations.

('randomly') distributed around the sphere, but instead also share the north and shallow ChRM direction as found in the underlying flow-unit (Fig. 5). This can be explained by two possibilities: (1) the breccia is magnetically overprinted, perhaps owing to syn-magmatic hydrothermal alteration, although the flow directions are primary; or (2) the entire Ganaams region was overprinted subsequent to emplacement of the lava. The former is preferred, because of the minor yet significant distinction in ChRM directions between site JP1133 (both

coherent lava and breccia clasts) v. the remainder of the Ganaams sites (Fig. 6). A secondary regional magnetic overprint would be expected to eliminate such distinctions.

In the type locality at Guperas Farm, site JP1142 shows significant ChRM scatter and a primary site direction was unobtainable; however, site JP1143 resulted in a stable remanence direction coinciding with that of the interbedded sedimentary sequence (see below). The Guperas Farm section is steeply dipping (slightly overturned; Table 2), so that a
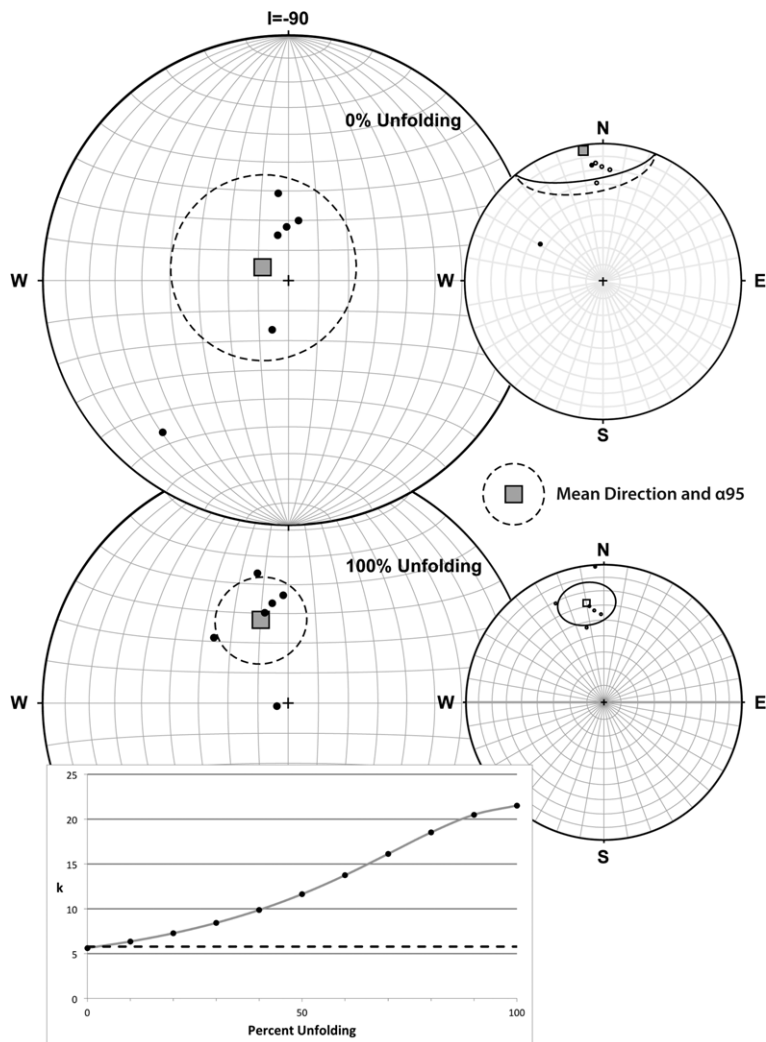

Fig. 6. Characteristic remanent magnetization directions, plotted on equal-area projections, from all of the samples in Guperas lava flows. All data are presented in geographic (0% unfolded) and tilt-corrected (100% unfolded) coordinates. The stereonets have been rotated 90° about the east–west axis, in order to cluster the data in the centre of the diagram, so that 0° inclination runs horizontally along centre of the projection (Allmendinger *et al.* 2013; Cardozo & Allmendinger 2013). The dashed line on the partial unfolding plot represents 95% statistical significance from the pre-folded precision values.

fold test is permitted between it and the shallowly dipping Ganaams sites. Correction for tectonic tilts at 100% increases the clustering of data from a precision of $k = 5.6$ to $k = 21.5$ (Fig. 6), thus constituting a positive fold test for the Guperas igneous rocks (the k ratio of 3.84 exceeds the 95% critical value of 3.72 for $N = 6$; Fisher *et al.* 1987, p. 219). Maximum precision is obtained at 110% rather than 100% unfolding, but we attribute this to coincidental alignment of directional scatter caused by

palaeosecular variation of the Mesoproterozoic geodynamo. Angular dispersion of the six site-mean virtual geomagnetic poles (VGPs) from Guperas Formation igneous rocks is 12.4°, consistent with the best-fit angular dispersion curve at *c.* 15° palaeolatitude from a quality-filtered global dataset of 1.0–2.2 Ga igneous rocks (Smirnov *et al.* 2011); this supports the notion that our dataset successfully averages palaeosecular variation of the Mesoproterozoic geodynamo. The mean of the six
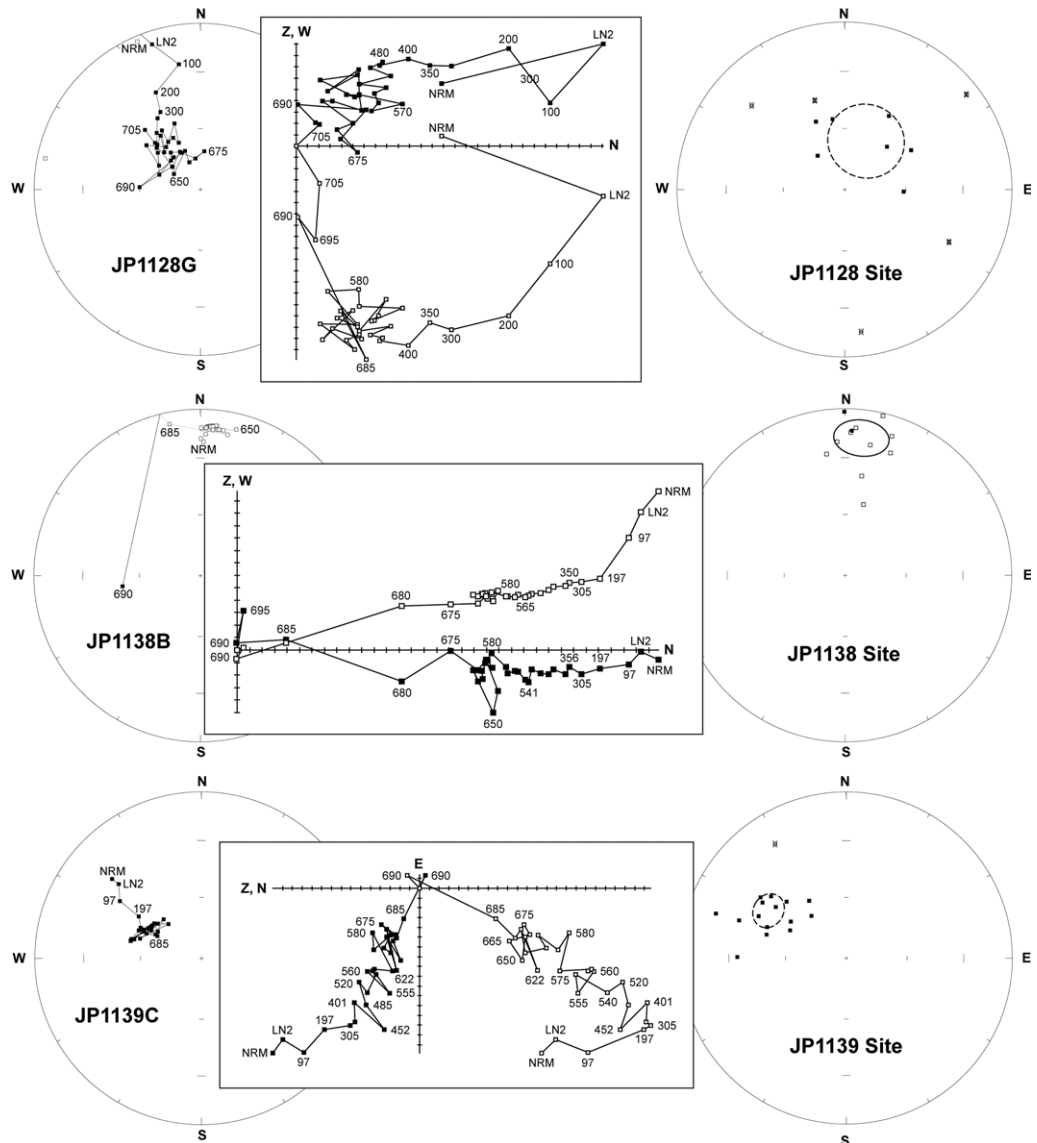

Fig. 7. Typical demagnetization behaviour for Guperas Formation sedimentary sections. Symbols and abbreviations as in Figure 5, but in addition, sample remanence directions excluded from the mean calculation are denoted by 'X' on the site-summary stereonets.

Guperas lava VGPs generates a palaeomagnetic pole at 72.0° N, 351.3° E, with Fisher (1953) statistics $K = 72.3$, $A_{95} = 7.9°$. Our results are similar to those presented by Piper (1975), using mainly blanket alternating field demagnetization to 30 mT.

Guperas sedimentary sections

Guperas Formation sedimentary rocks were collected at three localities and range in lithology from red siltstones and mudstones to coarse-grained sandstones with conglomerate. Conglomerate tests were conducted at two additional localities discussed below (Watson 1956). Most of the samples from the sedimentary localities showed good stability to thermal demagnetization (Fig. 7). All localities showed a low-unblocking-temperature overprint of the recent geomagnetic field (north-up) that is readily distinguishable from the dominantly north-shallow ChRM, dominated by unblocking
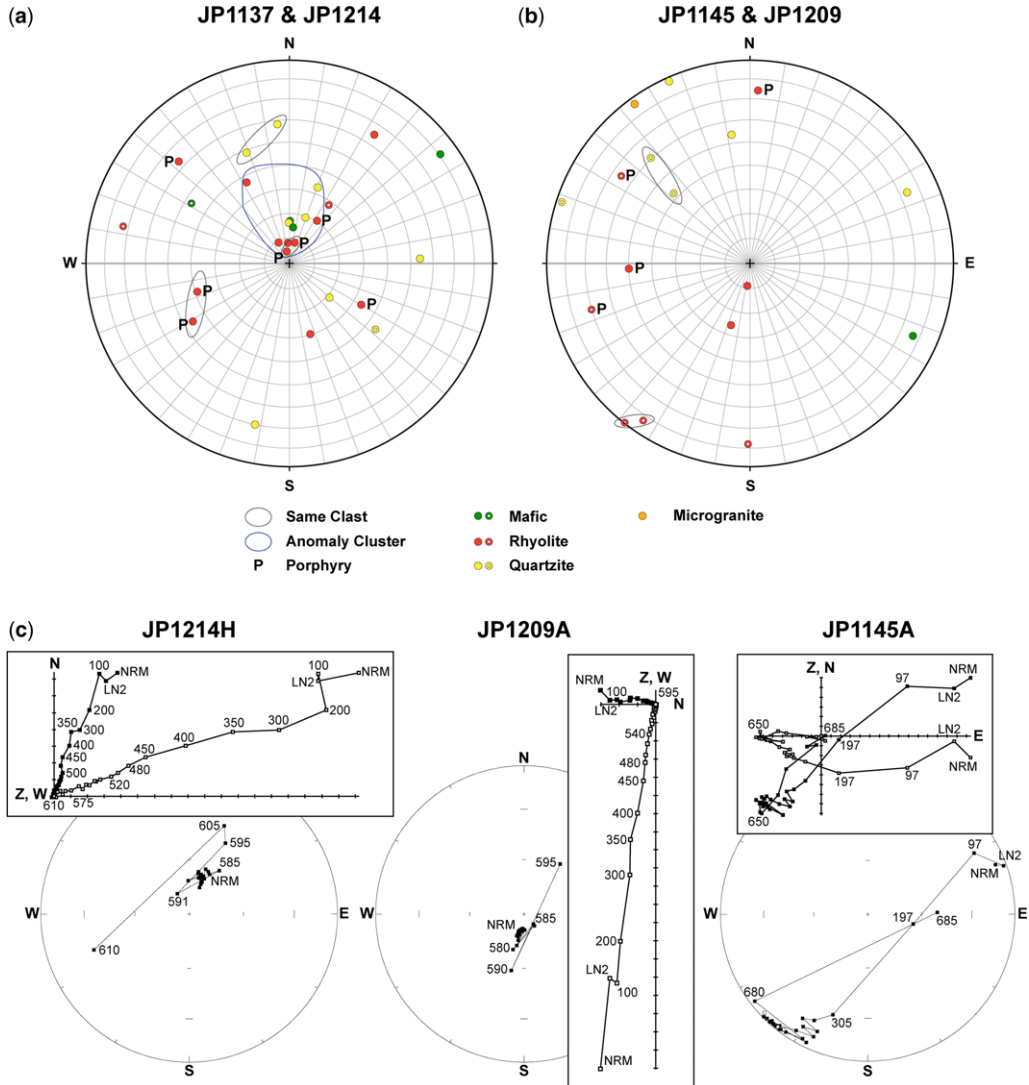
Fig. 8. Results of conglomerate tests in the Guperas Formation, all shown in geographic coordinates. In (**a**) and (**b**), equal-area stereographs follow the same symbol convention as in Figure 6. In (**c**), representative specimen demagnetization behaviours follow the same conventions as in Figure 5. Pairs of data encircled in grey indicate doubly sampled clasts for consistency tests. Data encircled by blue represent data that have a steep, north-down overprint direction.

Table 3. *Summary of palaeomagnetic data from the Guperas Formation conglomerate localities JP1137/1214 and JP1145/1209*

Locality				Geographic coordinates					
Code	Latitude (°S)	Longitude (°E)	Temperature (°C)	D (deg)	I (deg)	α_{95} (deg)	Lithology	R	R_0
JP1137	−25.709	016.682						4.43	5.35
A			571	332.8	80.6	1.8	Rhyolite		
B			595	252.9	50.9	3.2	Rhyolite porphyry		
C			595	239.0	43.9	11.3	Rhyolite porphyry		
D			595	282.6	−17.4	8.9	Rhyolite		
E			522	033.4	25.1	9.6	Rhyolite		
F			552	119.9	56.5	6.9	Rhyolite porphyry		
G			552	033.0	69.6	3.3	Rhyolite porphyry		
H			595	127.5	−45.7	2.2	Quartzite grit		
J			540	020.5	57.2	5.7	Quartzitic graywhacke		
K			571	312.7	26.9	4.5	Rhyolite porphyry		
L			595	034.0	−61.6	9.1	Rhyolite		
JP1214	−25.709	016.682						6.27	5.10
A			550	348.2	41.2	10.8	Purple quartzitic sandstone		
A			680	087.9	35.9	20.1	Purple quartzitic sandstone		
B			555	005.6	32.3	16.8	Purple quartzitic sandstone		
B			670	192.0	20.0	6.1	Purple quartzitic sandstone		
C			585	000.9	73.0	1.9	Mafic		
C			670	054.1	09.2	19.0	Mafic		
D			591	355.7	81.8	1.9	Rhyolite		
E			550	332.3	54.0	5.5	Rhyolite		
E			605	163.5	60.3	8.0	Rhyolite		
F			595	014.4	81.4	1.2	Rhyolite porphyry		
G			591	347.5	85.1	0.8	Rhyolite porphyry		
H			591	019.2	70.5	2.1	Quartzite		
I			540	359.1	73.7	3.6	Quartzite		
I			581	130.4	68.9	6.5	Quartzite		
J			570	006.0	75.5	5.0	Mafic		
J			585	301.6	−42.9	3.8	Mafic		
							Combined	10.34	7.40
JP1145	−25.672	016.608						3.28	4.57
A			685	218.4	−00.5	5.3	Rhyolite		
B			685	214.4	−07.4	5.8	Rhyolite		
C			685	002.5	15.6	4.3	Rhyolite porphyry		
D			565	153.3	01.0	4.4	Microgranite		
D			675	324.1	03.2	13.5	Microgranite		
E			675	113.9	13.7	3.4	Mafic		
F			541	344.2	26.6	11.0	Rhyolite porphyry		
F			685	267.8	40.0	4.5	Rhyolite porphyry		
G			585	304.3	−24.1	2.5	Rhyolite porphyry		
I			675	254.0	−19.8	5.5	Porphyry		
JP1209	−25.672	016.608						3.02	4.84
A			595	188.4	81.2	1.4	Rhyolite		
C			556	338.5	15.4	8.0	Quartzite		
C			700	336.0	01.8	8.0	Quartzite		
D			695	065.4	16.4	7.4	Quartzite		
E			700	180.8	−12.4	2.5	Rhyolite		
F			595	197.7	64.2	17.1	Rhyolite		
G			700	351.7	35.9	13.2	Quartzite		
H			570	288.2	−02.7	10.7	Quartzite		
I			665	312.7	−47.4	13.3	Quartzite		
J			695	316.8	−29.1	12.8	Quartzite		
							Combined	5.73	6.65

Table follows same conventions as Table 2. Temperature denotes the dominant demagnetization unblocking temperature step for the least-squares line-fitted ChRM component. Lithology describes the composition of the sampled clasts. Results for Watson's (1956) test for randomness are included by individual sample locality based on field season and a combined result based on locality. R, length of resultant vector; R_0, critical value for an equal-sized uniform distribution at 95% confidence. Shaded lines were not included in the randomness determination.

temperatures in the range of the Neél temperature of stoichiometric hematite (*c.* 680°C). All sections were sampled stratigraphically, over sections with thicknesses ranging from 23 to *c.* 75 m in hope of constructing magnetostratigraphies through the Guperas Formation, but the presence of only a single magnetic polarity within our dataset suggests that sedimentation was either relatively rapid or occurred during a period when geomagnetic reversals were infrequent.

Clasts from two conglomerate localities were sampled during two separate field seasons. The sites JP1137 and JP1214 are from the same locality, as are the sites JP1145 and JP1209. Most of the sampled clasts were either igneous (primarily felsic) rocks, or quartzitic sandstones. It is possible that these clasts are sourced from older Guperas strata, or from the older Barby, Kunjas or Nagatis Formations. The JP1145/JP1209 locality shows uniform ('random') scatter among the ChRM directions,
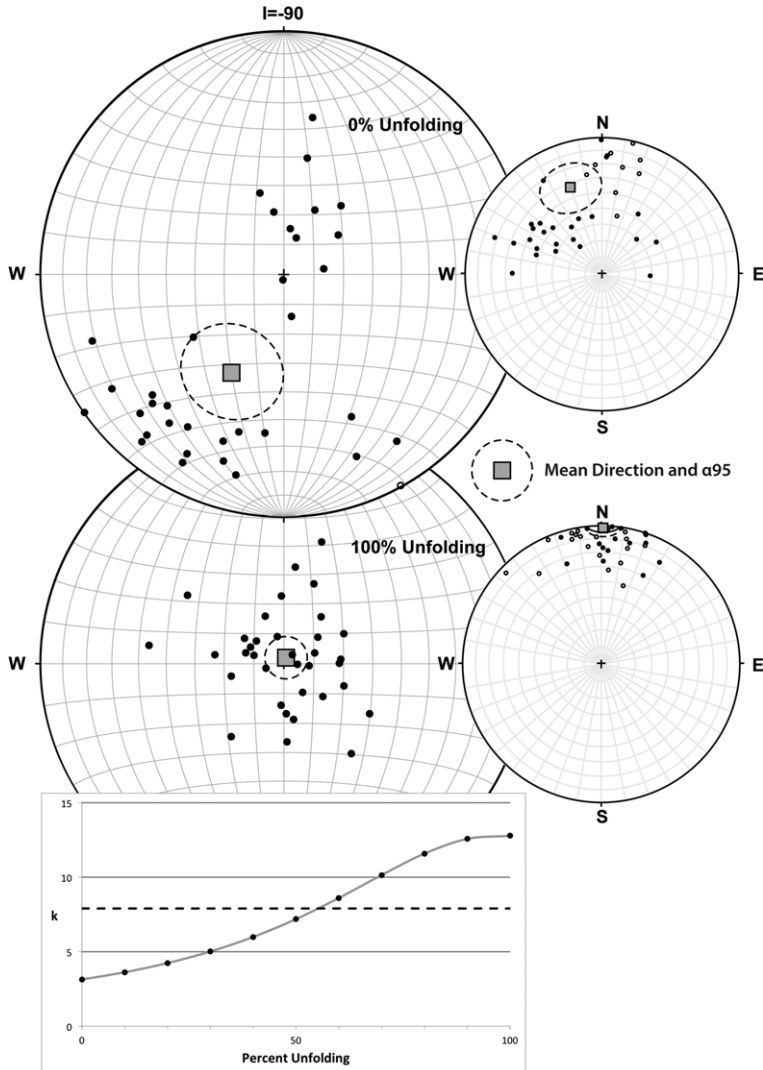

Fig. 9. Characteristic remanent magnetization directions, plotted on equal-area projections, from all of the Guperas sedimentary sections. All data are presented in geographic (0% unfolded) and tilt-corrected (100% unfolded) coordinates. Maximum clustering of data happens at 100% unfolding. Symbols follow same convention as in Figure 6. The stereonets have been rotated 90° about the east–west axis, in order to cluster the data in the centre of the diagram, so that 0° inclination runs horizontally along centre of the projection (Allmendinger *et al.* 2013; Cardozo *et al.* 2013). The dashed line on the partial unfolding plot represents 95% statistical significance from the pre-folded precision values.

with internal reproducibility of directions within two of the clasts (Fig. 8, Table 3) that passes Watson's (1956) test for randomness for both JP1145 and JP1209 individually and with combined datasets. The JP1137/JP1214 locality shows a similar range of directional scatter among ChRM vectors, including within-clast reproducibility, but that site also exhibits a cluster of moderate unblocking-temperature (spanning 200–600°C)

remanence directions to the north and steeply downward (Fig. 8, Table 3). JP1137 passes Watson's test for randomness, but neither JP1214 nor the combined dataset passes the randomness test. The partial overprint recorded at the JP1137/JP1214 locality is of unknown origin; its direction lies on the Devonian–Carboniferous part of the Gondwana apparent polar wander path (McElhinny et al. 2003; Torsvik et al. 2012), although no significant
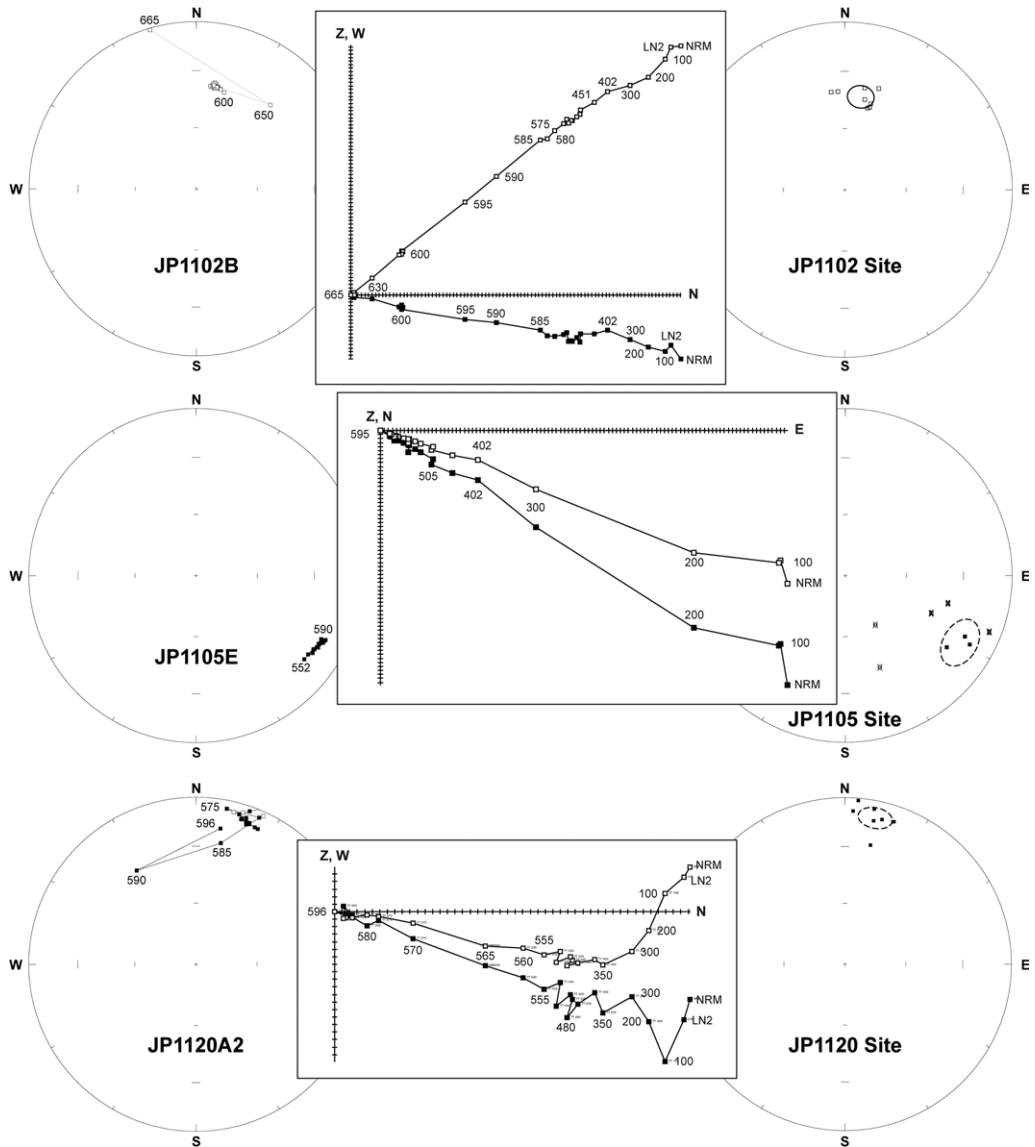

Fig. 10. Typical demagnetization behaviour for post-Guperas dyke intrusions. Each panel follows the same symbol convention as Figure 5.

Table 4. *Summary of palaeomagnetic data from the post-Guperas dyke localities, Sinclair region, Namibia*

	Locality				Geographic coordinates			VGP			
Code	Latitude (°S)	Longitude (°E)	Age (Ma)	n/N	D (deg)	I (deg)	α_{95} (deg)	Latitude (°N)	Longitude (°E)	K	A_{95} (deg)
Northern region											
JP1111	−25.453	016.586		8/8	022.7	06.2	16.2	53.9	057.5		
JP1112	−25.454	016.587		5/8	015.9	01.1	5.6	59.8	049.6		
JP1113	−25.454	016.587		6/8	013.2	−11.3	5.9	66.6	051.4		
JP1114	−25.483	016.581		8/8	003.7	−00.5	5.7	64.5	025.2		
JP1115	−25.483	016.582		8/8	010.8	08.5	4.7	58.5	037.5		
JP1116	−25.483	016.582		8/8	291.9	28.4	9.7	12.3	310.1		
JP1117	−25.483	016.582		8/8	347.7	−09.3	14.8	66.1	345.0		
Cluster A											
JP1118	−25.483	016.584		6/6	357.1	−33.3	5.7	82.2	355.8		
JP1119	−25.483	016.584		6/8	009.9	−35.1	10.6	79.0	074.8		
Cluster A	−25.483	016.584			003.4	−34.4		82.7	042.8		
JP1120	−25.483	016.586		8/8	011.7	11.1	6.5	56.9	038.3		
JP1121	−25.482	016.586		8/8	357.6	04.6	4.6	62.1	011.5		
JP1122	−25.482	016.586		6/8	011.8	01.9	3.4	61.2	041.7		
JP1123	−25.483	016.587		5/6	005.6	−38.6	15.9	83.7	071.8		
JP1124	−25.483	016.587		8/8	290.7	−31.5	14.1	25.5	279.0		
JP1125	−25.493	016.611		6/8	352.4	30.0	13.9	47.8	005.7		
JP1126	−25.497	016.627		6/8	009.4	−07.7	3.6	66.6	040.8		
JP1127	*−25.492*	*016.632*	*1105.22 ± 0.51*	*8/8*	*160.5*	*−42.8*	*12.4*	*36.2*	*354.6*		
JP1110	−25.506	016.621		7/8	260.7	−37.2	10.6	−00.9	084.0		
Cluster B											
JP1108	−25.510	016.624		7/8	354.1	18.8	13.3	54.4	006.6		
JP1109	−25.510	016.624		8/8	339.0	16.9	4.8	50.2	343.0		
Cluster B	−25.510	016.624			346.5	18.0		52.9	354.2		
Southern Region											
JP1131	−25.708	016.574		7/8	346.4	−44.1	9.2	77.8	282.9		
JP1132	−25.708	016.574			Lightning						
JP1103	−25.715	016.619			Lightning						
JP1104	−25.726	016.596			Lightning						

				n/N	Dec	Inc	a95					
JP1105	−25.713	016.639		3/8	120.3	21.1	10.1	31.9	289.6			
JP1147	*−25.714*	*016.639*		*4/8*	*207.0*	*07.7*	*12.1*	*56.1*	*071.0*			
Cluster C												
JP1107	−25.713	016.639		5/8	002.1	−27.7	12.8	78.8	027.2			
JP1148	−25.714	016.639		5/5	017.4	−35.5	9.9	72.8	089.4			
JP1149	−25.715	016.639		8/8	011.7	−23.6	6.7	72.7	058.3			
JP1150	−25.715	016.639		8/8	016.3	−20.7	5.5	68.5	065.4			
JP1151	−25.714	016.638		8/8	016.0	−41.9	6.0	75.4	104.0			
JP1152	−25.714	016.638		6/8	035.1	−31.0	15.1	56.2	098.3			
Cluster C	−25.714	016.639			016.3	−30.4	10.1	72.2	078.2			
JP1156	−25.711	016.646		Scattered								
Cluster D												
JP1157	−25.711	016.646		7/8	022.5	−21.2	4.8	64.1	076.1			
JP1158	−25.711	016.646		7/8	012.8	−16.3	6.6	68.8	053.9			
Cluster D	−25.711	016.646			017.6	−18.8		66.8	065.9			
JP1153	−25.714	016.647		Lightning								
Cluster E												
JP1154	−25.714	016.647		6/8	005.7	−16.8	12.3	72.0	035.2			
JP1155	−25.714	016.647		7/8	013.9	−17.3	9.6	68.6	057.2			
Cluster E	−25.714	016.647			009.8	−17.1		70.6	047.1			
JP1211	−25.711	016.646		7/8	032.6	12.4	17.7	45.0	065.9			
JP1144	*−25.713*	*016.672*		*8/8*	*181.1*	*−54.2*	*4.6*	*29.5*	*017.7*			
JP1141	−25.710	016.681		Scattered								
JP1140	−25.710	016.682	1105.54 ± 0.73	8/8	357.0	10.3	7.5	59.0	010.9			
JP1216	−25.710	016.682		6/8	340.4	39.2	27.6	38.5	353.3			
JP1217	−25.711	016.681		8/8	024.9	28.8	4.9	42.3	050.0			
JP1101	*−25.725*	*016.579*		*4/6*	*183.7*	*04.8*	*11.9*	*66.4*	*025.8*			
Cluster F												
JP1102	−25.726	016.596		8/8	009.8	−43.0	5.9	81.1	104.0			
JP1204	−25.726	016.596		8/8	014.2	−42.0	3.6	77.0	103.0			
JP1206	−25.726	016.597		8/8	017.5	−30.4	7.2	71.2	080.1			
Cluster F	−25.726	016.596			014.0	−38.5	11.7	76.6	092.0			
Mean	*N = 26*			**285/327**	**007.4**	**01.8**	**8.9**	**10.1**	**62.3**	**031.9**	**17.7**	**6.9**

Table follows the same conventions as Table 2. Sites that are dark grey are not in mean calculations, text that is only italicized indicates a site of opposite polarity to the modal direction, and light grey shades indicate site clusters.

Table 5. *Kalahari and Sinclair palaeomagnetic poles shown in Figure 12. Q is the reliability factor of Van der Voo (1990)*

Rock name	Code	Age (Ma)	Latitude (°N)	Longitude (°E)	A_{95} (deg)	1	2	3	4	5	6	7	Q	Reference(s)
Namaqua Eastern Zone	NEZ	<1165 ± 10	45	022	13	0	1	1	1	0	0	0	3	Evans *et al.* (2002), Pettersson *et al.* (2007)
Umkondo grand mean	UMK	1110 ± 3	64	039	4	1	1	1	1	1	1	1	7	Gose *et al.* (2006)
Guperas Lavas	GLAV		76	334	10	0	1	1	1	1	0	1	5	This study
Guperas Sediments	GSED		65	019	6	0	1	1	1	1	0	1	5	This study
All Guperas	GUP		74	357	9	0	1	1	1	1	0	1	5	This study
Post-Guperas Dykes	PGD	1105 ± 1	62	032	7	1	1	1	1	1	1	1	7	This study
Aubures Formation	AUB	<1108 ± 9	56	018	11	0	1	1	1	1	1	0	5	Kasbohm *et al.* (2015)
Kalkpunt Formation	KPT	≤1093 ± 7	57	003	7	1	0	1	0	1	0	0	3	Briden *et al.* (1979), Pettersson *et al.* (2007)
Central Namaqua belt	CNM	1030–1000	08	330	10	1	1	1	0	0	1	0	4	Onstott *et al.* (1986), Powell *et al.* (2001)
Port Edward Charnockite	PEC	1004 ± 5	−07	330	4	1	1	1	0	0	0	0	3	Gose *et al.* (2004)

Phanerozoic tectonic activity is recognized in the Sinclair region. Regardless, steep north-down directions are not observed at any other Guperas palaeomagnetic sites in the area, so the partial remagnetization with that direction is only local in scope.

Most pertinently, the typical north-shallow ChRM direction from Guperas igneous and sedimentary rocks is not observed at the two conglomerate localities, in which at least the redbed quartzite clast compositions are similar to the sampled Guperas strata. Therefore, with regard to the modal Guperas north-shallow ChRM direction, our two intraformational conglomerate tests are positive, indicating no regional remagnetization subsequent to conglomerate deposition. In addition to this constraint on the age of Guperas magnetization, conglomerate localities within the younger Aubures Formation redbeds also show large scatter of ChRM vectors from clasts that probably derive from the Guperas Formation (Kasbohm *et al.* 2015).

A fold test was implemented using both site-based and sample-based statistics based on an F-distribution comparison of precision, k, value significance levels (Table 2; McElhinny 1964). Partial unfolding of the Guperas sediments is shown in Figure 9. The overall precision is highest at 100% tilt-correction; the peak precision parameter is 4.13 times greater than that of the *in-situ* dataset, far exceeding the 95% confidence level of 1.62 for $N = 35$ samples (Fisher *et al.* 1987, p. 219). The fold test indicates that the remanence direction was obtained prior to deformation. The structures deforming Guperas strata are truncated by the unconformably overlying Aubures Formation (*c.* 1100–1090 Ma; Kasbohm *et al.* 2015); thus the fold test reported herein provides a strong constraint on the age of magnetization of Guperas sedimentary rocks.

Using the results for 100% untilting of all Guperas sedimentary samples, we compute a palaeomagnetic pole at 65.3° N, 018.7° E, with statistical precision $K = 19.3$ and $A_{95} = 5.7°$ (Table 2). These are the first high-quality results presented on the Guperas Formation sedimentary strata and broadly agree with the Guperas lava flow data presented by Piper (1975) and herein (above). The difference between igneous and sedimentary datasets is primarily in inclination, with the tilt-corrected sedimentary mean inclination ($-2°$) substantially shallower than that of the igneous rocks ($-28°$) However, because sedimentary section-mean ChRM vectors have both positive and negative inclinations, applying correction factors for inclination shallowing (King 1955) only serves to disperse the data, while keeping the overall mean inclination low. Therefore, no inclination correction is applied to the sedimentary data. Combining data from Guperas igneous

and sedimentary rocks at the site/locality levels, we obtain a 100% tilt-corrected directional mean of $D = 355.9°$, $I = -11.1°$, $k = 19.7$, $A_{95} = 11.9°$ ($N = 9$ localities) that does not include the use of Piper's (1975) results. The corresponding mean of VGPs produces a palaeomagnetic pole at 69.8° N, 004.1° E, $K = 49.1$, $A_{95} = 7.4°$. Following the Van der Voo (1990) seven-point quality scale, our results satisfy five of the criteria: statistics of the pole (#2), vector analysis (#3), positive field stability tests (#4), structural control (#5) and dissimilarity to younger poles (#7). The criteria not satisfied by this study are rock age (#1) and dual polarity of remanence (#6). Despite the lack of a direct numerical age constraint for the Guperas igneous rocks, their stratigraphic position in the Sinclair sequence is clearly defined (older than the 1105 Ma post-Guperas dykes, younger than the stratigraphically underlying Barby lavas) and thus they can contribute to a sequential apparent polar wander path for the Sinclair region.

Post-Guperas dykes

The post-Guperas dykes intrude both the Barby and Guperas formations, trending NE/SW and north/south in the southern and northern regions, respectively. However, the dykes have not been found to intrude the overlying Aubures Formation, indicating that they were intruded prior to Aubures sedimentation. Both mafic and rhyolitic dykes are present, the latter group including quartz– and feldspar–phyric porphyries. Some dykes are composite, with mafic margins and rhyolitic interiors.

The dykes exhibited excellent stability to thermal demagnetization (Fig. 10). Generally, within each sample the NRM consisted of either a single vector component, or a low-unblocking-temperature component parallel to the present field at the sampling locality, followed by a higher-stability component with magnetite unblocking temperatures greater than 550°C (rarely as high as *c.* 670°C coinciding with hematite). The clustering of remanence within sites varied (Fig. 10), but typically had a range of Fisher (1953) k-parameters between 20 and 150 (median $k = 69$ among sites included in the overall mean; Table 4). The high-unblocking-temperature ChRM direction of most of the dykes is concentrated to the north and shallow. Sites JP1101, 1127, 1144 and 1147 have the opposite polarity of ChRM, shallowly south-directed. Given that the two dated dykes with indistinguishable *c.* 1105.5 Ma U–Pb zircon ages have opposite polarities (site JP1140 with the north-shallow direction and site JP1127 with the south-shallow direction), averaging of the two polarities into a single mean direction and palaeomagnetic pole is appropriate (Tables 4 & 5). Although dyke

strikes vary systematically between our northern sampling region, where strikes are approximately north–south, and our southern sampling region, where strikes are approximately NE–SW, there is no significant difference in ChRM declination between the two areas (Table 4). Therefore, the
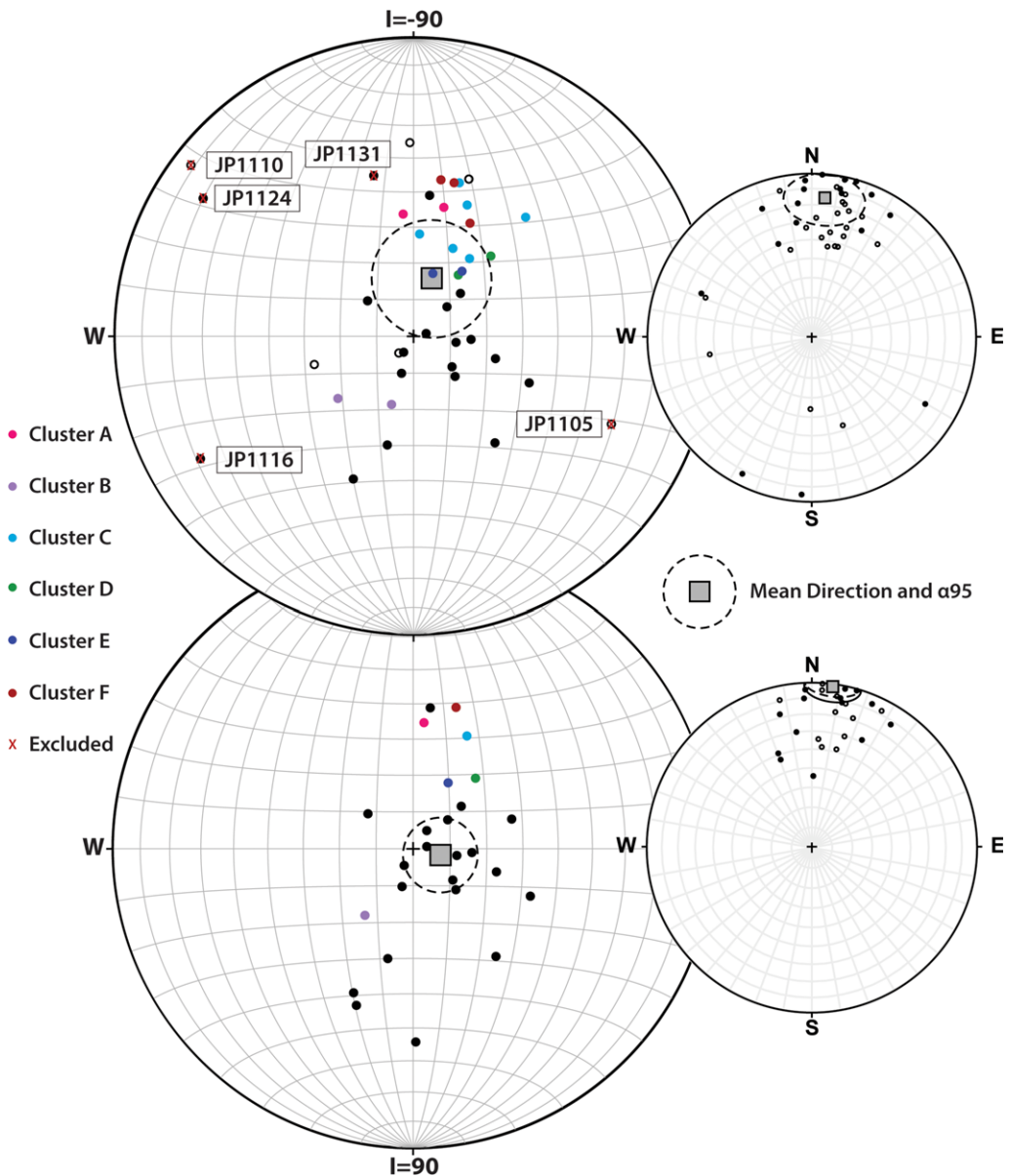

Fig. 11. (Top) Magnetic remanent directions for all post-Guperas dyke sampling localities using the same conventions as Figure 6. Sampling localities excluded from pole position computation are marked with a red X. (Bottom) Dyke localities were combined in 'clusters' of sites with similar remanent magnetization that are within 300 m of each other: cluster A (JP1118 and 1119); cluster B (JP1108 and 1109); cluster C (JP1107, 1148–1152); cluster D (JP1157 and 1158); cluster E (JP1154 and 55); Cluster F (JP1102, 1104, 1106). The stereonets have been rotated 90° about the east–west axis, in order to cluster the data in the centre of the diagram, so that 0° inclination runs horizontally along centre of the projection (Allmendinger *et al.* 2013; Cardozo *et al.* 2013). The dashed line on the partial unfolding plot represents 95% statistical significance from the pre-folded precision values.

variation in dyke trends is a primary feature of their emplacement. Sites JP1105, 1110, 1116, 1124 and 1131 show ChRM directions that deviate from the shallow north–south ChRM axis, oriented to the west; it is not clear whether these anomalous directions represent geomagnetic excursions or emplacement ages substantially different from *c.* 1105 Ma.

Sites JP1103, 1104, 1132, 1141, 1153 and 1156 show large scatter, probably due to lightning (most recognizable as single-component behaviour of an unusually strong NRM) or perhaps other mineralogical alterations.

A baked-contact field stability test (BCT) was performed on a rhyolite dyke intruding the Barby
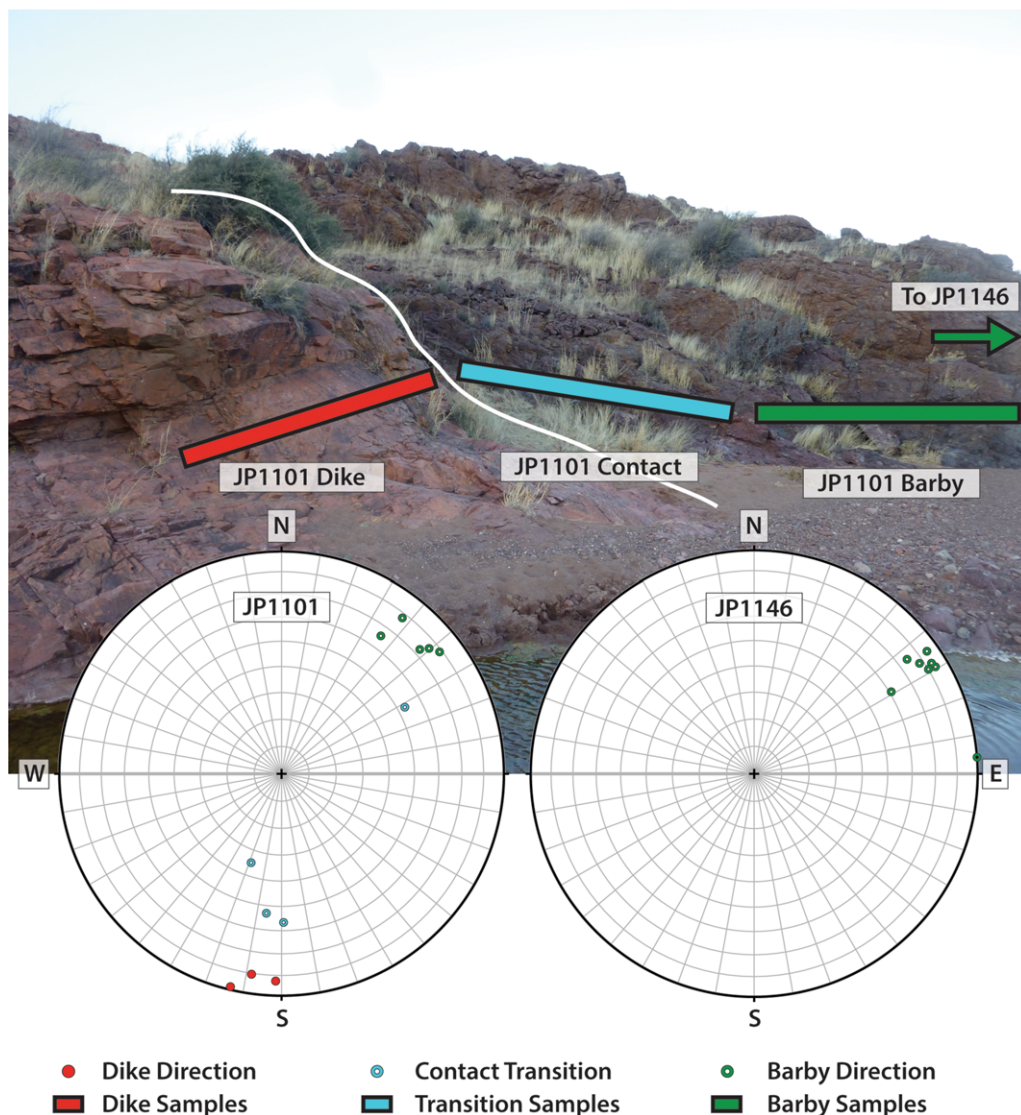
Fig. 12. Baked-contact test at JP1101 and JP1146 between intruding rhyolite dyke and Barby Formation host rock with field photograph, with the white line showing the contact between the two. The equal area stereographs use the same conventions as Figure 6, in geographic coordinates, and the colours indicate the dyke direction in the rhyolite (red), the transitional contact in the Barby Formation (light blue), and host Barby Formation (green). Rectangular bars indicate the sampling span of each segment of the baked contact test associated with different directional properties, with the green arrow indicating that JP1146 was sampled just outside the field image.

Formation at site JP1101. The ChRM direction of the dyke shows a south and shallow direction. Barby Formation host rocks near the dyke's contact show a transitional direction similar to that of the dyke ChRM, but more distant Barby rocks show a distinctly different NE and shallow direction (Fig. 12). Hessert (2014) reported results from this locality, and other Barby-dyke BCTs. The results reported herein indicate a positive BCT, implying that the north–south-shallow magnetization dates from the time of emplacement of the post-Guperas dykes at *c.* 1105.5 Ma.

Several post-Guperas dyke sites were located in close proximity to each other, with distinctive ChRM vectors suggestive of rapid local emplacement of parallel intrusions. In order to avoid biasing of the mean direction by such spatiotemporal clustering, we adopted the following procedure. If post-Guperas dyke sites were within 300 m of each other and had similar and distinctive remanent directions, an average direction was determined for each cluster (Fig. 11, Table 4). We identified six such dyke clusters and treated each as a statistical unit equal in weight to each of the other sites. With $N = 26$ dyke localities after clustering spatiotemporal binning, we determined a palaeomagnetic pole at 62.3° N, 031.9° E, with statistical precision $K = 17.7$, and $A_{95} = 6.9°$. Our post-Guperas dyke pole satisfies all seven of the Van der Voo (1990) quality criteria: rock age is known (#1); good statistics of the pole (#2); vector analysis (#3); positive conglomerate test in a nearby host rock and BCTs (#4); structural control (#5);

dual polarity of remanence (#6); and dissimilarity to younger poles (#7).

Discussion

The new palaeomagnetic poles presented in this study are close to those not only from earlier studies of the Sinclair region (Piper 1975), but also a companion reinvestigation of the overlying Aubures redbeds (Kasbohm *et al.* 2015). Most importantly, our Sinclair poles are indistinguishable from nearly coeval poles derived from autochthonous Kalahari craton; in particular, our new post-Guperas dykes pole is nearly identical to the grand mean pole from the Umkondo large igneous province (Gose *et al.* 2006; Figure 13, Table 5). These results suggest that the Sinclair terrane was autochthonous to the Kalahari craton at *c.* 1105 Ma. Miller (2008, 2013) presented a tectonic model in which the Sinclair terrane was joined to the Kalahari craton as early as *c.* 1330 Ma, and our data are consistent with that model. However, because of the lack of robust palaeomagnetic data for parts of the Sinclair terrane older than *c.* 1105 Ma, the possibility remains that significant displacement occurred between the terrane and the craton margin at one or more times in the interval between *c.* 1330 and *c.* 1105 Ma.

As our post-Guperas dyke data include precise U–Pb ages, our results can provide important constraints on the reversal history of the late Mesoproterozoic geodynamo. Hanson *et al.* (2004) suggested
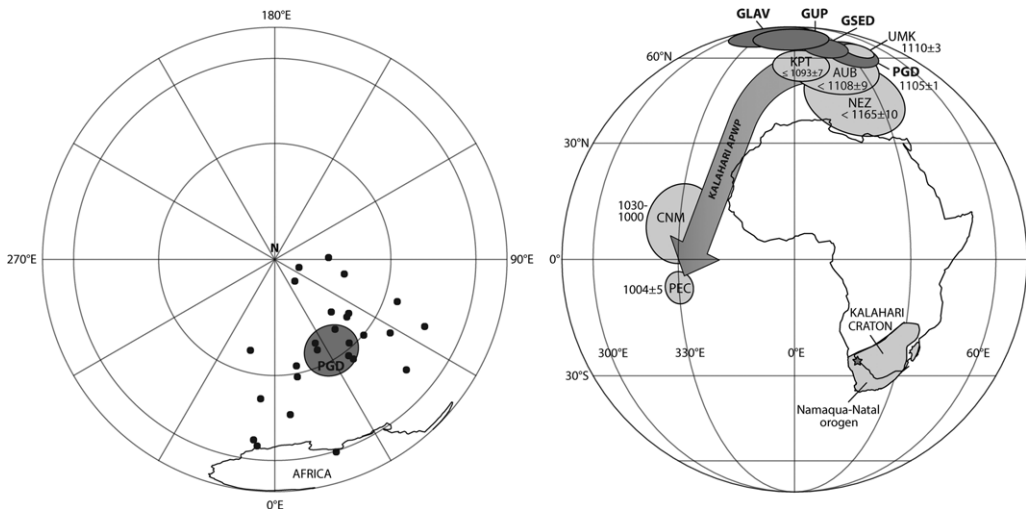

Fig. 13. (Left) VGP positions for dyke sites and clusters with mean pole in grey. (Right) Apparent polar wander path (APWP) for the Kalahari craton between *c.* 1200 and 1000 Ma (orthographic projection). Pole codes are explained in Table 5. Ages in Ma. Star, Sinclair sampling region.

that the vast majority of Umkondo magmatism (with shallow southward directions) occurred during an interval of Reversed geomagnetic polarity, coincident with the same polarity in the oldest magmatic units of the Keweenawan Mid-Continent Rift of Laurentia. Kasbohm *et al.* (2015) found the same southward-dominant remanence from Aubures Formation redbeds that are younger than 1108 ± 9 Ma, and reinterpreted that polarity as Normal (relative to the Keweenawan convention). Our new U–Pb ages from the post-Guperas (and pre-Aubures) dykes further refine Aubures sedimentation to younger than 1105 Ma, and lend support to the polarity choice of Kasbohm *et al.* (2015). The dominant polarity of remanence direction from the post-Guperas dykes is northward, which would correspond to Reversed polarity in the new interpretation. The dominant R → N transition observed in upper Sinclair strata thus mirrors the same dominant R → N transition in Keweenawan rocks of Laurentia. Our documented presence of dual magnetic polarity among post-Guperas dykes at 1105.5 Ma either dates precisely a single R → N transition through that interval, or that several geomagnetic reversals occurred prior to the advent of dominant north polarity during late Keweenawan and Aubures time.

The new data presented herein provide a basis for further palaeomagnetic studies of older parts of the Sinclair terrane. Broad similarity of our palaeomagnetic poles between the Guperas Formation and post-Guperas dykes suggests that the former unit is not substantially older than the latter (1105.5 Ma). Age constraints on the next older stratigraphic unit, the Barby Formation, are lax, although the preliminary Barby palaeomagnetic pole reported by Piper (1975) is also similar to those of the Guperas Formation and post-Guperas dykes – perhaps suggesting a Barby age also not substantially older than 1105.5 Ma. However, such a conclusion would contradict the traditional correlation of Barby with the lithologically similar Haiber Flats Formation in the Awasib Mountains, intruded by granites dated at *c.* 1215 Ma (Hoal & Heaman 1995). Regardless, positive outcomes of the BCTs between post-Guperas dykes and host Barby Formation lavas bode well for future palaeomagnetic studies in the Sinclair region, which have the potential to contribute substantially to Mesoproterozoic tectonic models of the Sinclair terrane and Kalahari craton at both regional and global scales.

References

ALLMENDINGER, R. W., CARDOZO, N. C. & FISHER, D. 2013. *Structural Geology Algorithms: Vectors & Tensors*. Cambridge University Press, Cambridge.

BECKER, T., GAROEB, H., LEDRU, P. & MILESI, J.-P. 2005. The Mesoproterozoic event within the Rehoboth Basement Inlier of Namibia: review and new aspects of stratigraphy, geochemistry, structure and plate tectonic setting. *South African Journal of Geology*, **108**, 465–492.

BECKER, T., SCHREIBER, U., KAMPUNZU, A. B. & ARMSTRONG, R. 2006. Mesoproterozoic rocks of Namibia and their plate tectonic setting. *Journal of African Earth Sciences*, **46**, 112–140.

BORG, G. 1988. The Koras–Sinclair–Ghanzi rift in southern Africa. Volcanism, sedimentation, age relationships and geophysical signature of a late Middle Proterozoic rift system. *Precambrian Research*, **38**, 75–90.

BOWRING, J. F., MCLEAN, N. M. & BOWRING, S. A. 2011. Engineering cyber infrastructure for U-Pb geochronology: tripoli and U–Pb_Redux. *Geochemistry Geophysics Geosystems*, **12**, Q0AA19, http://doi.org/10.1029/2010GC003479

BRIDEN, J. C., DUFF, B. A. & KRÖNER, A. 1979. Paleomagnetism of the Koras Group, Northern Cape Province. South Africa. *Precambrian Research*, **10**, 43–57.

CARDOZO, N. & ALLMENDINGER, R. W. 2013. Spherical projections with OSXStereonet. *Computers & Geosciences*, **51**, 193–205, http://doi.org/10.1016/j.cageo.2012.07.021

CORNELL, D. H., THOMAS, R. J., MOEN, H. F. G., REID, D. L., MOORE, J. M. & GIBSON, R. L. 2006. The Namaqua–Natal province. *In*: JOHNSON, M. R., ANHAEUSSER, C. R. & THOMAS, R. J. (eds) *The Geology of South Africa*. Geological Society of South Africa/Council for Geoscience, Johannesberg, 325–379.

CORNELL, D. H., VAN SCHIJNDEL, V., SIMONSEN, S. L. & FREI, D. 2015. Geochronology of Mesoproterozoic hybrid intrusions in the Konkiep Terrane, Namibia, from passive to active continental margin in the Namaqua–Natal Wilson Cycle. *Precambrian Research*, **265**, 166–188.

CORNER, B. 2008. The crustal framework of Namibia derived from an integrated interpretation of geophysical and geological data. *In*: MILLER, R. McG. (ed.) *The Geology of Namibia*. Geological Survey of Namibia, Windhoek, **1**, 2-1–2-19.

DALZIEL, I. W. D., MOSHER, S. & GAHAGAN, L. M. 2000. Laurentia–Kalahari collision and the assembly of Rodinia. *Journal of Geology*, **108**, 499–513.

EVANS, D. A. D., BEUKES, N. J. & KIRSCHVINK, J. L. 2002. Paleomagnetism of a lateritic paleoweathering horizon and overlying Paleoproterozoic red beds from South Africa: implications for the Kaapvaal apparent polar wander path and a confirmation of atmospheric oxygen enrichment. *Journal of Geophysical Research*, **107**, http://doi.org/10.1029/2001JB000432

FISHER, R. 1953. Dispersion on a Sphere. *Proceedings of the Royal Society, London A*, **217**, 295–305.

FISHER, N. I., LEWIS, T. & EMBLETON, B. J. J. 1987. *Statistical Analysis of Spherical Data*. Cambridge University Press, Cambridge.

GERSTENBERGER, H. & HAASE, G. 1997. A highly effective emitter substance for mass spectrometric Pb isotope ratio determinations. *Chemical Geology*, **136**, 309–312, http://doi.org/10.1016/S0009-2541(96)00033-2

GOSE, W. A., JOHNSTON, S. T. & THOMAS, R. J. 2004. Age of magnetization of Mesoproterozoic rocks from the Natal sector of the Namaqua–Natal belt, South Africa. *Journal of African Earth Sciences*, **40**, 137–145.

GOSE, W. A., HANSON, R. E., DALZIEL, I. W. D., PANCAKE, J. A. & SEIDEL, E. K. 2006. Paleomagnetism of the 1.1 Ga Umkondo large igneous province in southern Africa. *Journal of Geophysical Research – Solid Earth*, **111**, B09101.

HANSON, R. E. 2003. Proterozoic geochronology and tectonic evolution of southern Africa. *In*: YOSHIDA, M. & WINDLEY, B. E. & DASGUPTA, S. (eds) *Proterozoic East Gondwana: Supercontinent Assembly and Breakup.* The Geological Society, London, Special Publications, **206**, 427–463

HANSON, R. E., CROWLEY, J. L. ET AL. 2004. Coeval large-scale magmatism in the Kalahari and Laurentian cratons during Rodinia assembly. *Science*, **304**, 1126–1129.

HESSERT, J. 2014. *Paleomagnetic Baked-contact Tests in the Mesoproterozoic Sinclair region of Namibia*, BS thesis. Yale University.

HOAL, B. G. 1987. Terrane significance of the boundary between the Rehoboth and Gordonia subprovinces in southern Namibia. *Proceedings and Abstracts of the Alex L. du Toit Golden Jubilee Conference on Tectonostratigraphic Terrane Analysis*, Precambrian Research Unit, University of Cape Town, 42–45.

HOAL, B. G. 1989. The geological history of the Awasib Mountain terrain and its relationship to the Sinclair Sequence and Namaqualand Metamorphic Complex. *Communications of the Geological Survey of Namibia*, **5**, 41–51.

HOAL, B. G. 1993. The Proterozoic Sinclair Sequence in southern Namibia: intracratonic rift or active continental margin setting? *Precambrian Research*, **63**, 143–162.

HOAL, B. G. & HEAMAN, L. M. 1995. The Sinclair Sequence: U–Pb age constraints from the Awasib Mountain area. *Communications of the Geological Survey of Namibia*, **10**, 83–91.

HORSTMANN, U. E., AHRENDT, H., CLAUER, N. & PORADA, H. 1990. The metamorphic history of the Damara Orogen based on K/Ar data of detrital white micas from the Nama Group, Namibia. *Precambrian Research*, **48**, 41–61.

JACOBS, J., THOMAS, R. J. & WEBER, K. 1993. Accretion and indentation tectonics at the southern edge of the Kaapvaal craton during the Kibaran (Grenville) orogeny. *Geology*, **21**, 203–206.

JACOBS, J., PISAREVSKY, S., THOMAS, R. J. & BECKER, T. 2008. The Kalahari craton during the assembly and dispersal of Rodinia. *Precambrian Research*, **160**, 142–158.

JAFFEY, A. H., FLYNN, K. F., GLENDENIN, L. E., BENTLEY, W. C. & ESSLING, A. M. 1971. Precision measurements of half-lives and specific activities of ^{235}U and ^{238}U. *Physics Review C*, **4**, 1889–1906.

KAMPUNZU, A. B., AKANYANG, P., MAPEO, R. B. M., MODIE, B. N. & WENDORFF, M. 1998. Geochemistry and tectonic significance of the Mesoproterozoic Kgwebe metavolcanic rocks in northwest Botswana: implications for the evolution of the Kibaran Namaqua–Natal belt. *Geological Magazine*, **135**, 669–683.

KASBOHM, J., EVANS, D. A. D., PANZIK, J. E., HOFMANN, M. & LINNEMANN, U. 2015. Palaeomagnetic and geochronological data from Late Mesoproterozoic redbed sedimentary rocks on the western margin of the Kalahari craton. *In*: LI, Z. X., EVANS, D. A. D. & MURPHY, J. B. (eds) *Supercontinent Cycles Through Earth History*. The Geological Society, London, Special Publications 424, First published online May 21, 2015, http://doi.org/10.1144/SP424.4

KING, R. F. 1955. The remanent magnetism of artificially deposited sediments. *Monthly Notices of the Royal Astronomical Society Geophysics, Supplement*, **7**, 115–134.

KROGH, T. E. 1973. A low contamination method for hydrothermal decomposition of zircon and extraction of U and Pb for isotopic age determination. *Geochimica Cosmochimica Acta*, **37**, 485–494.

KRÖNER, A. 1977. The Sinclair aulacogen – a late Proterozoic volcano-sedimentary association along the Namib Desert of southern Namibia (SWA). *Abstracts of the 9th Colloquium of African Geologists*, University of Göttingen, 82–83.

MATTINSON, J. M. 2005. Zircon U-Pb chemical abrasion ('CA-TIMS') method: combined annealing and multi-step partial dissolution analysis for improved precision and accuracy of zircon ages. *Chemical Geology*, **220**, 47–66, http://doi.org/10.1016/j.chemgeo.2005.03.011

MCELHINNY, M. W. 1964. Statistical significance of the fold test in palaeomagnetism. *Geophysical Journal International*, **8**, 338–340.

MCELHINNY, M. W., POWELL, C. M. & PISAREVSKY, S. A. 2003. Paleozoic terranes of eastern Australia and the drift history of Gondwana. *Tectonophysics*, **362**, 41–65.

MCLEAN, N. M., BOWRING, J. F. & BOWRING, S. A. 2011. An algorithm for U–Pb isotope dilution data reduction and uncertainty propagation. *Geochemistry Geophysics Geosystems*, **12**, Q0AA18, http://doi.org/10.1029/2010GC003478

MILLER, R. McG. 1969. The Auborus formation of the Bethanie District, South West Africa. *University of Cape Town, Precambrian Research Unit, Bulletin*, **2**.

MILLER, R. McG. 2008. The Konkiep group. *In*: MILLER, R. McG. (ed.) *The Geology of Namibia*. Geological Survey of Namibia, Windhoek, **1**, 8-2–8-68.

MILLER, R. McG. 2013. Review of Mesoproterozoic magmatism, sedimentation and terrane amalgamation in southwestern Africa. *South African Journal of Geology*, **115**, 417–448.

ONSTOTT, T. C., HARGRAVES, R. B. & JOUBERT, P. 1986. Constraints on the evolution of the Namaqua Province II: reconnaissance palaeomagnetic and ^{40}Ar/^{39}Ar results from the Namaqua Province and the Kheis Belt. *Transactions of the Geological Society of South Africa*, **89**, 143–170.

PETTERSSON, A., CORNELL, D. H., MOEN, H. F. G., REDDY, S. & EVANS, D. A. D. 2007. Ion-probe dating of 1.2 Ga collision and crustal architecture in the Namaqua-Natal Province of southern Africa. *Precambrian Research*, **158**, 79–92.

PIPER, J. D. A. 1975. The paleomagnetism of Precambrian igneous and sedimentary rocks of the orange river belt in South Africa and South West Africa. *Geophysics Journal of the Royal Astronomical Society*, **40**, 313–344.

POWELL, C. McA., JONES, D. L., PISAREVSKY, S. & WINGATE, M. T. D. 2001. Palaeomagnetic constraints on the position of the Kalahari craton in Rodinia. *Precambrian Research*, **110**, 33–46.

SMIRNOV, A. V., TARDUNO, J. A. & EVANS, D. A. D. 2011. Evolving core conditions ca. 2 billion years ago detected by paleosecular variation. *Physics of the Earth and Planetary Interiors*, **187**, 225–231.

TORSVIK, T. H., VAN DER VOO, R. *ET AL.* 2012. Phanerozoic polar wander, palaeogeography and dynamics. *Earth-Science Review*, **114**, 325–368.

VAN DER VOO, R. 1990. The reliability of paleomagnetic data. *Tectonophysics*, **184**, 1–9.

WATSON, G. S. 1956. A test for randomness of directions. *Geophysics Journal International*, **7**, 160–161.

WATTERS, B. R. 1974. Stratigraphy, igneous petrology and evolution of the Sinclair Group in southern South West Africa. *University of Cape Town, Precambrian Research Unit, Bulletin*, **16**.

WATTERS, B. R. 1977. The Sinclair group: definition and regional correlations. *Transactions of the Geological Society of South Africa*, **80**, 9–16.